

Network Response Regression for Modeling Population of Networks with Covariates

Jingfei Zhang ¹, Will Wei Sun ² and Lexin Li ³

^{1,2} *Department of Management Science, Miami Business School,
University of Miami, Miami, FL, 33146.*

³ *Department of Biostatistics and Epidemiology, School of Public Health,
University of California at Berkeley, Berkeley, CA, 94720.*

Abstract

Multiple-network data are fast emerging in recent years, where a separate network over a common set of nodes is measured for each individual subject, along with rich subject covariates information. Existing network analysis methods have primarily focused on modeling a single network, and are not directly applicable to multiple networks with subject covariates. In this article, we propose a new network response regression model, where the observed networks are treated as matrix-valued responses, and the individual covariates as predictors. The new model characterizes the population-level connectivity pattern through a low-rank intercept matrix, and the parsimonious effects of subject covariates on the network through a sparse slope tensor. We formulate the parameter estimation as a non-convex optimization problem, and develop an efficient alternating gradient descent algorithm. We establish the non-asymptotic error bound for the actual estimator from our optimization algorithm. Built upon this error bound, we derive the strong consistency for network community recovery, as well as the edge selection consistency. We demonstrate the efficacy of our method through intensive simulations and two brain connectivity studies.

KEY WORDS: Brain connectivity analysis; community detection; multiple networks; non-convex optimization; tensor decomposition.

1 Introduction

In the past decade, there has been an explosion of network data arising in a wide variety of application areas, including biology, finance, neurology, social science, among many others (Kolaczyk, 2009). The majority of existing network analyses, however, have been focusing on a single network. More recently, multiple-network data are fast emerging, in which a separate network over a common set of nodes is measured for each individual subject in a study. An example is brain connectivity analysis, which examines functional and structural brain architectures through neurophysiological measures of brain activities and synchronizations (Varoquaux and Craddock, 2013). A typical brain connectivity study collects imaging scans, for instance, functional magnetic resonance imaging, or diffusion tensor imaging, from multiple subjects. Based on the imaging scan, a network is constructed for each individual, with the nodes corresponding to a common set of brain regions, and the edges encoding functional or structural associations between the regions. In addition, the study also collects a set of subject features such as age, sex, cognition, motor, substance use and many other traits. A fundamental scientific question of interest is to characterize the brain connectivity network at the population level and to understand if and how such a connectivity pattern is affected by subject covariates such as age and sex. Network analysis methods designed for a single network are not directly applicable for this type of task, and there has been a relative paucity of network models for analyzing multiple-network data with subject covariates. In this article, we aim to fill this gap.

There is a large body of literature on statistical analysis of a single network. Examples include Holland et al. (1983); Hoff et al. (2002); Airoidi et al. (2008); Zhao et al. (2012); Sewell and Chen (2015); Zhang et al. (2016); Gao et al. (2018); Huang and Feng (2018). See also Kolaczyk (2009) and Goldenberg et al. (2010) for reviews and references therein. Even though methods for a single network provide useful guidance when modeling multiple networks, they are often not directly applicable. Besides, it is nontrivial to incorporate subject covariates into those models. More recently, there have emerged some multiple-network analysis methods. Durante et al. (2017) proposed a Bayesian mixture latent space model for a population of networks. Their model was flexible, but did not incorporate any subject covariates, and could be computationally very intensive. Wang et al. (2017) studied shared and individual specific structures of multiple networks; Zhang et al. (2018c) developed a tensor version of principal components analysis for multiple structural connectivity networks, then associated the extracted features with subject traits. Both work offered useful tools for

modeling multiple networks; nevertheless, they focused on unsupervised learning of network structures. Sun and Li (2017) developed a tensor response regression model that includes network response as a special case. However, the proposed model could only handle continuous responses and it imposed a different structure on the coefficients as our model. We also note that our work addresses a completely different problem as multi-layer network analysis, in which different types of relationships among the same set of nodes are observed (Paul and Chen, 2016; Salter-Townshend and McCormick, 2017).

In this article, we propose a novel network response generalized linear regression model for a collection of network-valued data with additional covariates. We represent the observed networks as matrix-valued response variables, and the individual covariates as predictors. We then adopt the form of generalized linear model (GLM), and formulate the population-level network structure, after a proper transformation, as the sum of two high-dimensional components. The first component is the intercept matrix and is assumed to possess a low-rank structure. The second component involves the slope coefficient tensor, which directly models the effects of covariates on the network structure and is assumed to be sparse. Both sparsity and low-rankness are commonly used low-dimensional structures in high-dimensional regressions (Chen et al., 2016). They provide crucial and effective dimension reduction tools for modeling high-dimensional data, by substantially reducing the number of free parameters and computational complexity. Moreover, they are scientifically plausible, and are frequently employed in neuroimaging and numerous other applications (Zhou et al., 2013; Chen et al., 2016; Sun and Li, 2017; Zhang and Han, 2018). Particularly, the low-rank structure on the intercept term connects our model with several prevalent network models, such as the stochastic blockmodel and the network latent factor model. We show that, when there is only a single network, our model includes those as special cases. As a result, our model is capable of detecting communities of network nodes, within which the nodes are densely connected and between which there are sparser connections. The sparsity structure on the slope component imposes that the covariate effects on brain connectivity concentrate on a relatively small number of regions. This is reasonable, as brain connections are energy consuming and biological units tend to minimize energy-consuming activities (Bullmore and Sporns, 2009). Sparsity also greatly improves interpretation of the resulting model. Given the model, we formulate its parameter estimation as a non-convex regularized optimization problem, and develop an efficient alternating gradient descent algorithm. We also derive the non-asymptotic error bound of the actual estimator from our optimization algorithm, as well

as the asymptotic properties of community detection and edge selection based on our model.

Our proposal makes some unique contributions. First, we develop a systematic and flexible approach to model multiple networks with covariates. It can be applied to a variety of network data, with continuous, binary or nonnegative integer edges. Moreover, even though we primarily focus in this article on undirected networks that are represented in the form of symmetric matrices, our method is applicable to directed networks in the form of asymmetric matrices as well. Actually, we derive both the optimization algorithm and the theoretical properties first for the asymmetric case, then extends to the symmetric case. Second, with the increasing availability of network data with rich subject phenotype information, we provide a timely response to help address a class of scientific problems with immense importance. Moreover, although our method is motivated by brain connectivity studies, it is potentially applicable to other multiple-network data applications. Third, we successfully establish some strong theoretical properties for our method. We obtain an explicit non-asymptotic error bound for the actual estimator, first for a general loss function, then for the GLM loss function. This error bound reveals an interesting interplay between the computational efficiency and the statistical rate of convergence. It shows that the computational error decays geometrically with the number of iterations, while the statistical error matches with the minimax lower bound under the GLM loss. Built on this error bound, we further establish the strong consistency of a community detection procedure based on our model, where the number of communities is allowed to grow sub-linearly with the size of the network. Strong consistency is generally considered to be the highest achievable level of community recovery accuracy (Gao et al., 2018). We also prove the selection consistency in that we can consistently identify the edges that are affected by covariates and exclude those that are not affected. We comment that the aforementioned theoretical analyses are highly nontrivial, as they involve the alternating gradient descent, the factorization of the low-rank component, the hard-thresholding operator for sparsity, and the non-quadratic form of the loss function.

Throughout this article, we employ the following notations. Let \circ denote the outer product, and $\mathbf{I}_{n \times n}$ denote the $n \times n$ identity matrix. For a vector $\mathbf{b} \in \mathbb{R}^{d_1}$, let \mathbf{b}_i denote its i th entry, $1 \leq i \leq d_1$, and let $\|\mathbf{b}\|_2$ denote its Euclidean norm. For a matrix $\mathbf{B} \in \mathbb{R}^{d_1 \times d_2}$, let \mathbf{B}_{ij} denotes its (i, j) th entry, and let $\mathbf{B}_{i\cdot}$ and $\mathbf{B}_{\cdot j}$ denote its i th row and j th column, $1 \leq i \leq d_1, 1 \leq j \leq d_2$. Let $\|\mathbf{B}\|_2$, $\|\mathbf{B}\|_*$, $\|\mathbf{B}\|_F$, and $\|\mathbf{B}\|_\infty$ denote its spectral norm, nuclear norm, Frobenius norm, and entry-wise infinity norm, respectively. Let $\text{SVD}_r(\mathbf{B})$ denote the rank- r singular value decomposition of \mathbf{B} such that $\text{SVD}_r(\mathbf{B}) = [\mathbf{U}, \mathbf{\Sigma}, \mathbf{V}]$, where $\mathbf{\Sigma} \in \mathbb{R}^{r \times r}$

is a diagonal matrix with the largest r singular values of \mathbf{B} on the diagonal in a decreasing order, and $\mathbf{U} \in \mathbb{R}^{d_1 \times r}$, $\mathbf{V} \in \mathbb{R}^{d_2 \times r}$ collect the corresponding left and right singular vectors, respectively. For a tensor $\mathcal{B} \in \mathbb{R}^{d_1 \times d_2 \times d_3}$, let \mathcal{B}_{ijk} denotes its (i, j, k) th entry, $\mathcal{B}_{ij\cdot}$ denote the (i, j) th tube fiber, and $\mathcal{B}_{\cdot\cdot k}$ denote the k th frontal slice, $1 \leq i \leq d_1, 1 \leq j \leq d_2, 1 \leq k \leq d_3$. Let $\|\mathcal{B}\|_F$ denote the tensor Frobenius norm, which is defined as $\|\mathcal{B}\|_F = \sqrt{\sum_{ijk} \mathcal{B}_{ijk}^2}$, and $\|\mathcal{B}\|_0$ denote the number of nonzero entries in \mathcal{B} . We define the tensor vector multiplication as $\mathcal{B} \times_3 \mathbf{b} = \sum_{k=1}^{d_3} \mathbf{b}_k \mathcal{B}_{\cdot\cdot k}$ for $\mathbf{b} \in \mathbb{R}^{d_3}$ and $\mathcal{B} \in \mathbb{R}^{d_1 \times d_2 \times d_3}$, and define the tensor matrix inner product as $\langle \mathcal{B}, \mathcal{B} \rangle = \sum_{ijk} \mathcal{B}_{ijk} \mathcal{B}_{ijk}$ for $\mathcal{B} \in \mathbb{R}^{d_1 \times d_2}$ and $\mathcal{B} \in \mathbb{R}^{d_1 \times d_2 \times d_3}$.

The rest of the article is organized as follows. Section 2 introduces our network response generalized linear regression model, and discusses its connection with some existing network models. Section 3 develops an efficient alternating gradient descent algorithm for model estimation. Section 4 investigates the theoretical properties of the estimator. Section 5 demonstrates the effectiveness of our method through simulations, and Section 6 applies our model to two studies of brain functional and structural connectivities.

2 Model

2.1 Network Response Model

Let $\mathcal{G}(\mathcal{V}, \mathcal{E})$ denote a network, where \mathcal{V} is the set of n nodes and \mathcal{E} is the set of edges. It can be uniquely represented by the corresponding $n \times n$ adjacency matrix \mathbf{A} , where $\mathbf{A}_{jj'}$ denotes the edge from node j to j' , $1 \leq j, j' \leq n$. For a symmetric network, $\mathbf{A}_{jj'} = \mathbf{A}_{j'j}$. For a binary network, $\mathbf{A}_{jj'} \in \{0, 1\}$, while for a count network, $\mathbf{A}_{jj'}$ is a nonnegative integer. We consider multiple networks, $\mathcal{G}_1(\mathcal{V}, \mathcal{E}_1), \dots, \mathcal{G}_N(\mathcal{V}, \mathcal{E}_N)$, observed from N individual subjects of a study. Here we assume all N networks share a common set of nodes V , and \mathcal{E}_i is the set of edges for the i th subject, $1 \leq i \leq N$. Let $\mathbf{A}^{(1)}, \dots, \mathbf{A}^{(N)}$ denote the corresponding adjacency matrices of $\mathcal{G}_1, \dots, \mathcal{G}_N$. Additionally, for each subject, we observe a vector of p covariates, denoted by $\mathbf{x}_i = (x_{i1}, \dots, x_{ip})^\top$. We assume the covariates are not perfectly correlated, in that any one covariate cannot be written as a linear combination of other covariates. Denote $\boldsymbol{\mu}^{(i)} = \mathbb{E}\{\mathbf{A}^{(i)} | \mathbf{x}_i\}$, where the expectation $\mathbb{E}(\cdot)$ is applied element-wise to the entries in $\mathbf{A}^{(i)}$. We postulate the following network response generalized linear regression model: $\mathbf{A}^{(i)}$ conditional on \mathbf{x}_i follows an exponential distribution with a canonical link function that

$$g\{\boldsymbol{\mu}^{(i)}\} = \boldsymbol{\Theta} + \mathcal{B} \times_3 \mathbf{x}_i, \quad i = 1, \dots, N, \quad (1)$$

where $g(\cdot)$ is a known and invertible link function and is applied element-wise to the entries of $\boldsymbol{\mu}^{(i)}$, $\boldsymbol{\Theta} \in \mathbb{R}^{n \times n}$ is the intercept matrix that characterizes the population level network connectivity, and $\boldsymbol{\mathcal{B}} \in \mathbb{R}^{n \times n \times p}$ is the slope tensor that encodes the effects of subject covariates on the network connectivity. We next specify our choices of $g(\cdot)$, $\boldsymbol{\Theta}$ and $\boldsymbol{\mathcal{B}}$. First, the choice of $g(\cdot)$ depends on the data type of $\mathbf{A}^{(i)}$. For instance, if the edges in $\mathbf{A}^{(i)}$ are binary, we choose a logit link function, $g(\mu) = \log\{\mu/(1 - \mu)\}$; if the edges in $\mathbf{A}^{(i)}$ are count data, we choose a log link function, $g(\mu) = \log(\mu)$. Second, we impose that $\boldsymbol{\Theta}$ follows a low-rank structure. This structure effectively reduces the number of free parameters. Moreover, it connects (1) with, and is also more flexible than, several commonly used network models, as we further discuss in Section 2.2. Third, we impose that $\boldsymbol{\mathcal{B}}$ is sparse, i.e., the effects of covariates concentrate only on a subset of connections. This sparsity assumption again reduces the number of free parameters, greatly facilitates the model interpretation, and is also well supported by empirical neurological studies (Vounou et al., 2010; Supekar et al., 2013). We briefly comment that, it is possible to impose more complex structures on $\boldsymbol{\Theta}$ and $\boldsymbol{\mathcal{B}}$, e.g., we may additionally require $\boldsymbol{\Theta}$ to be sparse, or $\boldsymbol{\mathcal{B}}$ to be low-rank. Even though these structures can be incorporated in our model framework with some straightforward modification, we choose to focus on the current setup as it offers a good balance between model complexity and model flexibility.

To ensure the low-rank structure of $\boldsymbol{\Theta}$, we adopt the idea of Burer-Monteiro factorization (Burer and Monteiro, 2003), in which the low-rank matrix is reparameterized as the product of two factor matrices, $\boldsymbol{\Theta} = \mathbf{U}\mathbf{V}^\top$, where $\mathbf{U}, \mathbf{V} \in \mathbb{R}^{n \times r}$, and r is the rank of $\boldsymbol{\Theta}$. This reparameterization avoids repeatedly performing the computationally expensive singular value decomposition, which is often required in optimization with the low-rank constraint. If the adjacency matrix is symmetric, we reparameterize $\boldsymbol{\Theta}$ as $\boldsymbol{\Theta} = \mathbf{U}\boldsymbol{\Lambda}\mathbf{U}^\top$, where $\mathbf{U} \in \mathbb{R}^{n \times r}$ and $\boldsymbol{\Lambda}$ is a $r \times r$ diagonal matrix with diagonal entries $\{-1, 1\}$. If $\boldsymbol{\Theta}$ is positive semi-definite, then $\boldsymbol{\Lambda}$ becomes the identity matrix. To enforce the sparsity of $\boldsymbol{\mathcal{B}}$, we adopt the hard-thresholding sparsity constraint, by setting $\|\boldsymbol{\mathcal{B}}\|_0 \leq s$ for some positive integer s . Compared to the lasso type soft-thresholding constraint, the hard-thresholding constraint reduces bias and has been shown to enjoy superior performance in many high-dimensional problems (Wang et al., 2015; Sun et al., 2017; Zhang et al., 2018a,b). In Section 3, we present an efficient optimization algorithm to estimate $\boldsymbol{\Theta}$ and $\boldsymbol{\mathcal{B}}$ under the low-rank and sparse constraints.

It is noteworthy that, based on the parameterization $\boldsymbol{\Theta} = \mathbf{U}\boldsymbol{\Lambda}\mathbf{U}^\top$, we can detect clusters, or communities, of nodes, so that the nodes are more densely connected within the

clusters and less so between the clusters. This is termed community detection, and is one of the fundamental problems in network data analysis. There is a long line of research on community detection; see Zhao (2017) for a review. Assuming the nodes in the network form several communities and the community structure is fully determined by Θ , we recover the community labels by treating each row of \mathbf{U} as a sample, then clustering the rows.

2.2 Connections with Existing Network Models

Before turning to parameter estimation, we show that our proposed model (1), when applied to a single network, reduces to several prevalent network models, including the stochastic blockmodel (Holland et al., 1983), the network latent space model (Hoff et al., 2002), and the network latent factor model (Hoff, 2009). To establish these connections, we focus on a single network $\mathcal{G}(\mathcal{V}, \mathcal{E})$, with the adjacency matrix \mathbf{A} , and $\boldsymbol{\mu} = \mathbb{E}(\mathbf{A})$.

The stochastic blockmodel (Holland et al., 1983) is one of the most popular network models. It imposes that the nodes form a number of, say, K , communities, and the edges are determined by the community memberships of the two end nodes and are independent given the community assignment. Accordingly, the model can be written as

$$g(\boldsymbol{\mu}) = \mathbf{C}\mathbf{M}\mathbf{C}^\top,$$

where $\mathbf{C} \in \mathbb{R}^{n \times K}$ is the binary community assignment matrix with $\mathbf{C}_{jk} = 1$ if node j belongs to the k th community and 0 otherwise, and $\mathbf{M} \in \mathbb{R}^{K \times K}$ characterizes the connecting probabilities within and between the communities, $1 \leq j \leq n, 1 \leq k \leq K$. It is seen that the rank of the matrix $\mathbf{C}\mathbf{M}\mathbf{C}^\top$ is K , and as such this model can be viewed as a special case of model (1), in the sense that both postulate that the network pattern admits some low-rank structure.

The network latent space model (Hoff et al., 2002), also referred to as the latent position model, is another popular network model thanks to its easy interpretation; see Kim et al. (2017) for a review on this model. It assumes the nodes are positioned in a K -dimensional latent space, and two nodes are likely to form a tie if their latent positions are close to each other. One way to measure the closeness is the projection based distance. Then the model can be written as

$$g(\boldsymbol{\mu}) = \alpha \mathbf{1}_n \mathbf{1}_n^\top + \mathbf{C}(\mathbf{M}\mathbf{C})^\top,$$

where $\mathbf{1}_n$ is an n -dimensional vector of ones, $\mathbf{C} \in \mathbb{R}^{n \times K}$ has its j th row $\mathbf{c}_j^\top \in \mathbb{R}^{K \times 1}$ encoding the latent position of node j in the K -dimensional latent space, $\mathbf{M} \in \mathbb{R}^{n \times n}$ is a diagonal

matrix with its j th diagonal entry equal to $1/\|c_j\|$, $1 \leq j \leq n$. We see the rank of the matrix $\alpha \mathbf{1}\mathbf{1}^\top + \mathbf{C}(\mathbf{M}\mathbf{C})^\top$ is $(K + 1)$, and thus this model is again a special case of (1).

The network latent factor model (Hoff, 2009) is closely related to the latent space model. It can be written as

$$g(\boldsymbol{\mu}) = \boldsymbol{\alpha} \otimes \mathbf{1}_n^\top + \boldsymbol{\alpha}^\top \otimes \mathbf{1}_n + \mathbf{C}\mathbf{C}^\top,$$

where $\boldsymbol{\alpha} \in \mathbb{R}^n$ has its j th entry α_j encoding the additive effect, and $\mathbf{C} \in \mathbb{R}^{n \times K}$ has its j th row $\mathbf{c}_j^\top \in \mathbb{R}^{K \times 1}$ encoding the multiplicative effect. In this case, the rank of the matrix $\boldsymbol{\alpha} \otimes \mathbf{1}_n^\top + \boldsymbol{\alpha}^\top \otimes \mathbf{1}_n + \mathbf{C}\mathbf{C}^\top$ is again $(K + 1)$.

In the single network setup, compared to the above models, our model (1) is more general, in that it only assumes the low-rankness of the matrix $\boldsymbol{\Theta}$, but imposes no additional constraint on the network structure such as the block structure. Moreover, model estimation of the above models can be computationally intensive. For instance, in the stochastic blockmodel, the block membership for each node needs to be estimated, usually by a variational expectation-maximization (EM) approach. In the latent space model, the latent position of each node needs to be estimated, and the model is usually formulated within a Bayesian framework using Markov chain Monte (MCMC) type estimation. Such estimation procedures can be computationally expensive, and are generally difficult to apply for large networks when the number of nodes are in hundreds. For our model (1), we next develop an efficient alternating gradient descent algorithm that can easily handle networks with hundreds or more nodes.

3 Estimation

We propose to estimate the parameters $\boldsymbol{\Theta}$ and $\boldsymbol{\mathcal{B}}$ in model (1) through a non-convex regularized optimization. We first develop the optimization algorithm for the general asymmetric case, then for the symmetric case.

Denote the negative log-likelihood function of the network response model (1) by $\ell(\boldsymbol{\Theta}, \boldsymbol{\mathcal{B}})$, which, up to a constant, is of the form (McCullagh and Nelder, 1989),

$$\ell(\boldsymbol{\Theta}, \boldsymbol{\mathcal{B}}) = -\frac{1}{N} \sum_{i=1}^N \sum_{j \neq j'}^n \left[\mathbf{A}_{jj'}^{(i)} \boldsymbol{\eta}_{jj'}^{(i)} - \psi \left\{ \boldsymbol{\eta}_{jj'}^{(i)} \right\} \right], \quad (2)$$

where $\boldsymbol{\eta}^{(i)} = g\{\boldsymbol{\mu}^{(i)}\} = \boldsymbol{\Theta} + \boldsymbol{\mathcal{B}} \times_3 \mathbf{x}_i$, $i = 1, \dots, N$, and $\psi(\cdot)$ is the cumulant function with its first derivative $\psi'(\cdot) = g(\cdot)^{-1}$.

Algorithm 1 Optimization algorithm for (3)

Step 1 **initialization**: compute $\bar{\mathbf{A}} = \sum_{i=1}^N \mathbf{A}^{(i)}/N$, and perform singular value decomposition, $\text{SVD}_r\{g(\bar{\mathbf{A}})\} = [\bar{\mathbf{U}}_0, \bar{\mathbf{\Sigma}}_0, \bar{\mathbf{V}}_0]$. Set $\mathbf{U}^{(0)} = \bar{\mathbf{U}}_0 \bar{\mathbf{\Sigma}}_0^{1/2}$, $\mathbf{V}^{(0)} = \bar{\mathbf{V}}_0 \bar{\mathbf{\Sigma}}_0^{1/2}$, and $\mathbf{B}^{(0)} = \mathbf{0}$.

repeat

Step 2: update $\mathbf{U}^{(t+1)} = \mathbf{U}^{(t)} - \delta \nabla_{\mathbf{U}} \tilde{\ell} \left\{ \mathbf{U} \mathbf{V}^{(t)\top}, \mathbf{B}^{(t)} \right\} \Big|_{\mathbf{U}=\mathbf{U}^{(t)}}$;

Step 3: update $\mathbf{V}^{(t+1)} = \mathbf{V}^{(t)} - \delta \nabla_{\mathbf{V}} \tilde{\ell} \left\{ \mathbf{U}^{(t+1)} \mathbf{V}^\top, \mathbf{B}^{(t)} \right\} \Big|_{\mathbf{V}=\mathbf{V}^{(t)}}$;

Step 4: update $\mathbf{B}^{(t+1)} = \text{Truncate} \left[\mathbf{B}^{(t)} - \tau \nabla_{\mathbf{B}} \tilde{\ell} \left\{ \mathbf{U}^{(t+1)} \mathbf{V}^{(t+1)\top}, \mathbf{B} \right\} \Big|_{\mathbf{B}=\mathbf{B}^{(t)}, s} \right]$.

until the objective function converges.

For the general case that Θ is low-rank but not necessarily symmetric, we consider the factorization $\Theta = \mathbf{U} \mathbf{V}^\top$ and the corresponding optimization problem,

$$\min_{\substack{\mathbf{U}, \mathbf{V} \in \mathbb{R}^{n \times r} \\ \mathbf{B} \in \mathbb{R}^{n \times n \times p}}} \tilde{\ell}(\mathbf{U} \mathbf{V}^\top, \mathbf{B}), \quad \text{subject to} \quad \|\mathbf{B}\|_0 \leq s, \quad (3)$$

where we augment the loss function $\ell(\Theta, \mathbf{B})$ with an additional regularizer,

$$\tilde{\ell}(\mathbf{U} \mathbf{V}^\top, \mathbf{B}) = \ell(\mathbf{U} \mathbf{V}^\top, \mathbf{B}) + \frac{1}{8} \|\mathbf{U}^\top \mathbf{U} - \mathbf{V}^\top \mathbf{V}\|_F^2.$$

The regularizer $\|\mathbf{U}^\top \mathbf{U} - \mathbf{V}^\top \mathbf{V}\|_F^2/8$ is added to guarantee the uniqueness of the factorization of $\Theta = \mathbf{U} \mathbf{V}^\top$. Adding this term does not change the optimization problem, but merely reduces the set of solutions from all possible factorizations to the ones that are balanced in that $\sigma_i(\mathbf{U}) = \sigma_i(\mathbf{V}) = \sigma_i(\Theta)^{1/2}$, where $\sigma_i(\cdot)$ denotes the singular values of a matrix in a descending order, $i = 1, \dots, r$. Such a regularizer has been commonly employed in low-rank matrix factorization (Park et al., 2016; Zheng and Lafferty, 2016). In (3), the rank r and the sparsity s are two tuning parameters, and we will discuss their selection toward the end of this section. While the factorization $\Theta = \mathbf{U} \mathbf{V}^\top$ ensures the low-rank constraint for Θ , we adopt the hard-thresholding constraint $\|\mathbf{B}\|_0 \leq s$ to ensure the sparsity of \mathbf{B} . To enforce the sparsity along the solution path, we employ a truncation operator $\text{Truncate}(\mathbf{B}, s)$, which is defined as

$$[\text{Truncate}(\mathbf{B}, s)]_{jj'l} = \begin{cases} \mathbf{B}_{jj'l} & \text{if } (j, j', l) \in \text{supp}(\mathbf{B}, s), \\ 0 & \text{otherwise,} \end{cases}$$

for $\mathbf{B} \in \mathbb{R}^{d_1 \times d_2 \times d_3}$ and $s \leq d_1 d_2 d_3$. Here $\text{supp}(\mathbf{B}, s)$ is the set of indices of \mathbf{B} corresponding to its largest s absolute values. We then develop an alternating gradient descent algorithm for (3) to iteratively update \mathbf{U} , \mathbf{V} and \mathbf{B} . We summarize the optimization procedure in

Algorithm 2 Optimization algorithm for (4)

Step 1 **initialization**: solve the optimization problem (3) using Algorithm 1; denote the output of Algorithm 1 as $\tilde{\mathbf{U}}, \tilde{\mathbf{V}}, \tilde{\mathbf{B}}$, and set $\Lambda_{ii} = \text{sign}(\tilde{\mathbf{U}}_i^\top \tilde{\mathbf{V}}_i)$, $i = 1, \dots, r$, $\mathbf{U}^{(0)} = (\tilde{\mathbf{U}} + \Lambda \tilde{\mathbf{V}}^\top)/2$ and $\mathbf{B}^{(0)} = \tilde{\mathbf{B}}$.

repeat

Step 2: update $\mathbf{U}^{(t+1)} = \mathbf{U}^{(t)} - \delta \nabla_{\mathbf{U}} \ell \left\{ \mathbf{U} \Lambda \mathbf{U}^\top, \mathbf{B}^{(t)} \right\} \Big|_{\mathbf{U}=\mathbf{U}^{(t)}}$;

Step 3: update $\mathbf{B}^{(t+1)} = \text{Truncate} \left[\mathbf{B}^{(t)} - \tau \nabla_{\mathbf{B}} \ell \left\{ \mathbf{U}^{(t+1)} \Lambda \mathbf{U}^{(t+1)\top}, \mathbf{B} \right\} \Big|_{\mathbf{B}=\mathbf{B}^{(t)}, s} \right]$.

until the objective function converges.

Algorithm 1. In this algorithm, $\nabla_{\mathbf{U}} \tilde{\ell}(\mathbf{U}\mathbf{V}^\top, \mathbf{B})$ denotes the gradient of the objective function $\tilde{\ell}(\mathbf{U}\mathbf{V}^\top, \mathbf{B})$ with respect to \mathbf{U} , and $\nabla_{\mathbf{V}} \tilde{\ell}(\mathbf{U}\mathbf{V}^\top, \mathbf{B})$, $\nabla_{\mathbf{B}} \tilde{\ell}(\mathbf{U}\mathbf{V}^\top, \mathbf{B})$ are defined similarly. For simplicity, we fix the step size δ when updating \mathbf{U} and \mathbf{V} , and τ when updating \mathbf{B} . In Section 4, the theoretical conditions provide useful guidance on the magnitude of δ and τ to ensure the linear convergence rate of the algorithm, based on which we discuss their empirical choices. We stop the iterations when the difference of consecutive objective values is smaller than a threshold, say, 10^{-3} . Our empirical experience has suggested that this algorithm converges very fast, usually within 10 to 20 iterations.

Next, for the case that Θ is low-rank and symmetric, we consider the factorization $\Theta = \mathbf{U} \Lambda \mathbf{U}^\top$ and the corresponding optimization problem,

$$\min_{\substack{\mathbf{U} \in \mathbb{R}^{n \times r}, \Lambda \in \mathcal{D}_r \\ \mathbf{B} \in \mathbb{R}^{n \times n \times p}}} \ell(\mathbf{U} \Lambda \mathbf{U}^\top, \mathbf{B}), \quad \text{subject to} \quad \|\mathbf{B}\|_0 \leq s, \quad (4)$$

where \mathcal{D}_r denotes the set of all $r \times r$ diagonal matrices with diagonal entry values $\{-1, 1\}$. We again develop an alternating gradient descent algorithm for (4), and summarize it in Algorithm 2. In this algorithm, we have chosen not update the estimate of Λ . This is because we initialize by first solving the optimization problem (3), treating Θ as a general matrix without the symmetry constraint. From solving (3), the obtained $[\tilde{\mathbf{U}}; \tilde{\mathbf{V}}]$ consistently estimates $[\mathbf{U}^*; \Lambda \mathbf{U}^{*\top}]$, as we show in Theorem 1 in Section 4, where $\Theta^* = \mathbf{U}^* \Lambda \mathbf{U}^{*\top}$ is the true symmetric coefficient. As such, the diagonal entries of Λ can be accurately estimated using $\Lambda_{ii} = \text{sign}(\tilde{\mathbf{U}}_i^\top \tilde{\mathbf{V}}_i)$, $i = 1, \dots, r$.

The rank r and the sparsity s in (3) and (4) are two tuning parameters. We select these parameters via the eBIC criterion proposed in Chen and Chen (2012). Specifically, among a set of working ranks and sparsity levels, we choose the combination that minimizes

$$eBIC = 2N \times \ell(\hat{\Theta}, \hat{\mathbf{B}}) + [\log(n^2 N) + \log\{n^2(p+1)\}] \times (2nr + s),$$

where the loss function is as specified in (3), and $\hat{\Theta}, \hat{\mathcal{B}}$ are the estimates of Θ, \mathcal{B} under the working rank and sparsity level. The eBIC criterion with the loss function (4) can be calculated similarly. This criterion balances between model fitting and sparsity, and similar versions of this criterion have been employed in rank and sparsity tuning (Zhou et al., 2013; Sun et al., 2017).

4 Theory

We first derive the non-asymptotic error bound of the proposed estimator for a general loss function in Section 4.1. The results include the case without the symmetry constraint in Theorem 1, and the case with the symmetry constraint in Corollary 1. Built upon these results, we next derive the error bound for the GLM loss in Theorem 2 in Section 4.2. Finally, we obtain the community detection consistency and the selection consistency in Section 4.3.

4.1 Error Bound for a General Loss Function

We first introduce a set of regularity conditions. Let $\ell_g(\Theta, \mathcal{B})$ denote a general loss function defined with respect to a low-rank matrix $\Theta \in \mathbb{R}^{n \times n}$ and a sparse tensor $\mathcal{B} \in \mathbb{R}^{n \times n \times p}$, and is evaluated based on N sample observations. Let Θ^* denote the true coefficient matrix with rank r^* , and \mathcal{B}^* the true coefficient tensor with s^* nonzero entries. Let $\mathbb{B}_{\Theta^*}(\kappa_1) \subset \mathbb{R}^{n \times n}$ denote the Frobenius-norm ball around Θ^* with radius $\kappa_1 > 0$, and $\mathbb{B}_{\mathcal{B}^*}(\kappa_2) \subset \mathbb{R}^{n \times n \times p}$ the Frobenius-norm ball around \mathcal{B}^* with radius $\kappa_2 > 0$.

(A1) Assume that the loss function ℓ_g satisfies, with respect to Θ , the restricted strong convexity with parameter $\mu_1 > 0$, and the restricted strong smoothness with parameter $\alpha_1 > 0$, in that, for any $\mathcal{B} \in \mathbb{B}_{\mathcal{B}^*}(\kappa_2)$ with at most s nonzero entries and for any matrices $\Theta_1, \Theta_2 \in \mathbb{B}_{\Theta^*}(\kappa_1)$ with rank at most r ,

$$\frac{\mu_1}{2} \|\Theta_2 - \Theta_1\|_F^2 \leq \ell_g(\Theta_2, \mathcal{B}) - \ell_g(\Theta_1, \mathcal{B}) - \langle \nabla_{\Theta} \ell_g(\Theta_1, \mathcal{B}), \Theta_2 - \Theta_1 \rangle \leq \frac{\alpha_1}{2} \|\Theta_2 - \Theta_1\|_F^2.$$

(A2) Assume that the loss function ℓ_g satisfies, with respect to \mathcal{B} , the restricted strong convexity with parameter $\mu_2 > 0$, and the restricted strong smoothness with parameter $\alpha_2 > 0$, in that, for any $\Theta \in \mathbb{B}_{\Theta^*}(\kappa_1)$ with rank at most r and for any $\mathcal{B}_1, \mathcal{B}_2 \in \mathbb{B}_{\mathcal{B}^*}(\kappa_2)$ with at most s nonzero entries,

$$\frac{\mu_2}{2} \|\mathcal{B}_2 - \mathcal{B}_1\|_F^2 \leq \ell_g(\Theta, \mathcal{B}_2) - \ell_g(\Theta, \mathcal{B}_1) - \langle \nabla_{\mathcal{B}} \ell_g(\Theta, \mathcal{B}_1), \mathcal{B}_2 - \mathcal{B}_1 \rangle \leq \frac{\alpha_2}{2} \|\mathcal{B}_2 - \mathcal{B}_1\|_F^2.$$

(A3) For any Θ with rank at most r and \mathcal{B} with at most s nonzero entries, assume that

$$\begin{aligned} |\langle \nabla_{\Theta} \ell_g(\Theta^*, \mathcal{B}) - \nabla_{\Theta} \ell_g(\Theta^*, \mathcal{B}^*), \Theta \rangle| &\leq \kappa_N \|\Theta\|_F \cdot \|\mathcal{B} - \mathcal{B}^*\|_F, \\ |\langle \nabla_{\mathcal{B}} \ell_g(\Theta, \mathcal{B}^*) - \nabla_{\mathcal{B}} \ell_g(\Theta^*, \mathcal{B}^*), \mathcal{B} \rangle| &\leq \kappa_N \|\Theta - \Theta^*\|_F \cdot \|\mathcal{B}\|_F \end{aligned}$$

where $\kappa_N \in (0, 1)$ is the Lipschitz gradient parameter that depends on N .

(A4) For a tolerance parameter $\delta \in (0, 1)$, assume that there exist ϵ_N and ξ_N such that

$$\|\nabla_{\Theta} \ell_g(\Theta^*, \mathcal{B}^*)\|_2 \leq \epsilon_N \quad \text{and} \quad \|\nabla_{\mathcal{B}} \ell_g(\Theta^*, \mathcal{B}^*)\|_{\infty} \leq \xi_N,$$

hold with probability at least $1 - \delta$. Here ϵ_N and ξ_N depend on N and δ .

Conditions (A1) and (A2) require the loss function ℓ_g to have strong convexity and strong smoothness within some restricted regions. Condition (A3) requires ℓ_g to satisfy a form of the Lipschitz continuous gradient condition. Take the first inequality as an example, the gradient is taken with respect to the low-rank component, while the Lipschitz continuity condition is with respect to the sparse component. Note that (A3) is not a local condition, as it is defined over all $\{\Theta, \mathcal{B}\}$ in the parameter space. Condition (A4) requires the gradient of the loss function is upper bounded in terms of the spectral norm for the low-rank component and the infinity norm for the sparse component. These conditions are utilized in our population and sample-based analysis to tackle the non-convexity of the optimization problem. They are all reasonably mild assumptions, and similar conditions have often been imposed in numerous non-convex problems, e.g., Wang et al. (2014); Zhang et al. (2018b).

Next we establish the error bound for the actual estimator from Algorithm 1 where $\Theta = \mathbf{U}\mathbf{V}^{\top}$. Write the rank- r^* singular value decomposition of the true Θ^* as $\tilde{\mathbf{U}}^* \mathbf{\Sigma}^* \tilde{\mathbf{V}}^{*\top}$, where $\tilde{\mathbf{U}}^*, \tilde{\mathbf{V}}^* \in \mathbb{R}^{n \times r^*}$ are the left and right singular matrices, and $\mathbf{\Sigma}^* = \text{diag}(\sigma_1, \dots, \sigma_{r^*})$, where σ_i 's are the singular values of Θ^* such that $\sigma_1 \geq \dots \geq \sigma_{r^*} > 0$. Write $\mathbf{U}^* = \tilde{\mathbf{U}}^* (\mathbf{\Sigma}^*)^{1/2}$, $\mathbf{V}^* = \tilde{\mathbf{V}}^* (\mathbf{\Sigma}^*)^{1/2}$, and thus $\Theta^* = \mathbf{U}^* \mathbf{V}^{*\top}$. Write $\mathbf{M}^* = [\mathbf{U}^*; \mathbf{V}^*] \in \mathbb{R}^{(n+n) \times r^*}$. For $\mathbf{M} = [\mathbf{U}; \mathbf{V}] \in \mathbb{R}^{(n+n) \times r^*}$ and $\mathcal{B} \in \mathbb{R}^{n \times n \times p}$, define the distance metric,

$$D\{\mathbf{M}, \mathcal{B}\} = d^2(\mathbf{M}, \mathbf{M}^*) + \frac{1}{\sigma_1} \|\mathcal{B} - \mathcal{B}^*\|_F^2, \quad \text{where } d(\mathbf{M}, \mathbf{M}^*) = \min_{\mathbf{\Gamma} \in \mathbb{Q}_{r^*}} \|\mathbf{M} - \mathbf{M}^* \mathbf{\Gamma}\|_F,$$

and \mathbb{Q}_{r^*} denotes the set of $r^* \times r^*$ orthonormal matrices. The factor $1/\sigma_1$ in this distance metric comes from the difference between $\Theta = \mathbf{U}\mathbf{V}^{\top}$ and $\mathbf{M} = [\mathbf{U}; \mathbf{V}]$, as we have $\|\Theta - \Theta^*\|_F^2 \leq c\sigma_1 d^2(\mathbf{M}, \mathbf{M}^*)$ for some constant c . The next theorem gives a non-asymptotic error bound for the estimators $\mathbf{M}^{(t)} = [\mathbf{U}^{(t)}; \mathbf{V}^{(t)}]$ and $\mathcal{B}^{(t)}$ from Algorithm 1 at the t th iteration.

Theorem 1. Suppose the general loss function ℓ_g satisfies Conditions (A1)-(A4), with $\kappa_1 = \kappa_2 = \sqrt{\sigma_{r^*}}/3$. Let c_1 and c_2 be constants such that $c_1 \leq \min\{1/32, \mu_1/(192\alpha_1^2)\}$, and $6c_1\alpha_2 \leq c_2 \leq \min\left\{1/3, \sqrt{\mu_1'/(4 + 6\alpha_1 + 2/\mu_2)}\right\}$, where $\mu_1' = \min\{\mu_1, 2\}$. Let the step sizes $\delta = c_1/\sigma_1$, $\tau = c_2/\alpha_2$, and $s = \gamma s^*$, where $\gamma \geq 1 + \{(3\alpha_2 + \mu_2 c_2)/(\mu_2 c_2)\}^2$. Let the sample size N be large enough such that $r^* \phi_1 \epsilon_N^2 + s^* \phi_2 \xi_N^2 \leq (1 - \rho) c_2^2 \sigma_1 \sigma_{r^*}$ and $\kappa_N \leq \min\left\{\sqrt{\mu_1 \mu_2 / (48 c_1 \mu_1 + 96)}, \sqrt{c_1 \mu_1 \mu_2^2 / 8}\right\}$, where $\rho = \max\{1 - \delta \mu_1 \sigma_{r^*} / 16, 1 - \tau \mu_2 / 18\} \in (0, 1)$ is a contraction parameter, and ϕ_1 and ϕ_2 are constants that depend on c_1 , c_2 , γ , μ_1 , μ_2 , α_1 and α_2 . Then for a tolerance parameter $\delta \in (0, 1)$, for any initial estimator $\{\mathbf{M}^{(0)}, \mathbf{B}^{(0)}\}$ satisfying $D\{\mathbf{M}^{(0)}, \mathbf{B}^{(0)}\} \leq c_2^2 \sigma_{r^*}$, we have, with probability at least $1 - \delta$,

$$D\left\{\mathbf{M}^{(t)}, \mathbf{B}^{(t)}\right\} \leq \rho^t D\left\{\mathbf{M}^{(0)}, \mathbf{B}^{(0)}\right\} + \frac{r^* \phi_1 \epsilon_N^2 + s^* \phi_2 \xi_N^2}{(1 - \rho) \sigma_1}. \quad (5)$$

Theorem 1 portrays the estimation error at each iteration of our Algorithm 1. The right hand side of (5) consists of two terms. The first term corresponds to the computational error. The second term corresponds to the statistical error, in which $r^* \phi_1 \epsilon_N^2$ is related to the statistical error for the low-rank component estimation, and $s^* \phi_2 \xi_N^2$ is related to the statistical error for the sparse component estimation. This error bound reveals an interesting interplay between the computational efficiency and the statistical rate of convergence. Note that the computational error decays geometrically with the iteration number t , whereas the statistical error remains the same as t grows. Therefore, this bound provides a meaningful guidance for the maximal number of iterations. We see that, after $t \geq \log_\rho \left((r^* \phi_1 \epsilon_N^2 + s^* \phi_2 \xi_N^2) / [(1 - \rho) \sigma_1 D\{\mathbf{M}^{(0)}, \mathbf{B}^{(0)}\}] \right)$ iterations, the computational error is to be dominated by the statistical error. The resulting estimator then falls within the statistical precision of the true parameter.

We make a few remarks on the computational error. Later in Section 4.2 under the GLM loss function, we further remark on the statistical error. First, the computational error $\rho^t D\{\mathbf{M}^{(0)}, \mathbf{B}^{(0)}\}$ directly relies on the contraction parameter ρ , in that a smaller value of ρ leads to a faster convergence. When the step sizes δ and τ increase, ρ decreases. In addition, a greater σ_{r^*} indicates a stronger signal in the rank- r^* matrix, and when σ_{r^*} increases, ρ decreases. Second, the convexity parameters μ_1 and μ_2 reflect lower bounds on the ‘‘curvature’’ of the objective function around the true parameters. Therefore, a larger (μ_1, μ_2) implies a faster convergence. On the other hand, the smoothness parameters α_1 and α_2 reflect upper bounds on the ‘‘curvature’’ of the objective function around the true parameters. Henceforth, a larger (α_1, α_2) implies a slower convergence. Third, the

computational error is also a function of the initialization error $D\{\mathbf{M}^{(0)}, \mathbf{B}^{(0)}\}$. In Theorem 1, we require the initialization error to be bounded, i.e., the initial estimators are not too far away from the true parameters. This assumption is necessary to handle the non-convexity of the optimization, and has been often imposed in non-convex optimization (Wang et al., 2014; Sun et al., 2017; Zhang et al., 2018b).

Theorem 1 also provides some guidance on the choices of the step sizes δ and τ in Algorithm 1. To ensure the linear convergence rate, c_1 is upper bounded, and so is δ . Also, c_2 is both upper and lower bounded, and so is τ . In practice, if the convexity and smoothness parameters μ_1 , μ_2 , α_1 and α_2 can be calculated or roughly estimated for the loss function ℓ_g , the upper bounds for c_1 and c_2 can be obtained following Theorem 1. These upper bounds can then be used to choose δ and τ , along with a rough estimate of σ_1 . We may, for example, estimate σ_1 using the largest entry in the initial value $\bar{\Sigma}_0$ in Algorithm 1. Starting with some initial choices of δ and τ , one can update the step sizes depending on the empirical convergence of the algorithm.

We next consider the symmetric case, and obtain the error bound for the actual estimator from Algorithm 2 where $\Theta = \mathbf{U}\Lambda\mathbf{U}^\top$. We first write the rank- r^* eigen-decomposition of Θ^* as $\tilde{\mathbf{U}}^*\tilde{\Lambda}^*\tilde{\mathbf{U}}^{*\top}$, where $\tilde{\mathbf{U}}^* \in \mathbb{R}^{n \times r^*}$ is the matrix of eigenvectors, and $\tilde{\Lambda}^* = \text{diag}(\lambda_1, \dots, \lambda_{r^*})$, where λ_i 's are the eigenvalues of Θ^* such that $|\lambda_1| \geq |\lambda_2| \geq \dots \geq |\lambda_{r^*}|$. Then the singular values of Θ^* are $\sigma_i = |\lambda_i|, i = 1, \dots, r^*$. Write $\Lambda = \text{diag}(\text{sign}(\lambda_1), \dots, \text{sign}(\lambda_{r^*}))$ and $\mathbf{U}^* = \tilde{\mathbf{U}}^* \text{diag}(\sigma_1^{1/2}, \dots, \sigma_{r^*}^{1/2})$, we have $\Theta^* = \mathbf{U}^*\Lambda\mathbf{U}^{*\top}$. For $\mathbf{U} \in \mathbb{R}^{n \times r^*}$ and $\mathbf{B} \in \mathbb{R}^{n \times n \times p}$, define the distance metric,

$$D\{\mathbf{U}, \mathbf{B}\} = d^2(\mathbf{U}, \mathbf{U}^*) + \|\mathbf{B} - \mathbf{B}^*\|_F^2 / \sigma_1, \quad \text{where } d(\mathbf{U}, \mathbf{U}^*) = \min_{\Gamma \in \mathbb{Q}_r} \|\mathbf{U} - \mathbf{U}^*\Gamma\|_F,$$

and \mathbb{Q}_{r^*} is as defined before. The next lemma gives a non-asymptotic error bound for the estimators $\mathbf{U}^{(t)}$ and $\mathbf{B}^{(t)}$ from Algorithm 2 at the t th iteration.

Corollary 1. *Suppose the general loss function ℓ_g satisfies Conditions (A1)-(A4), with $\kappa_1 = \kappa_2 = \sqrt{\sigma_{r^*}}/3$. Let c_1 and c_2 be constants such that $c_1 \leq \mu_1/(96\alpha_1^2)$, and $3c_1\alpha_2 \leq c_2 \leq \min\{1/3, \sqrt{\mu_1/(9\alpha_1/2 + 8/\mu_2)}\}$. Let the step sizes $\delta = c_1/\sigma_1$, $\tau = c_2/\alpha_2$, and $s = \gamma s^*$, where $\gamma \geq 1 + \{(3\alpha_2 + \mu_2 c_2)/(\mu_2 c_2)\}^2$. Let the sample size N be large enough such that $r^* \phi_1 \epsilon_N^2 + s^* \phi_2 \xi_N^2 \leq (1 - \rho)c_2 \sigma_1 \sigma_{r^*}$ and $\kappa_N \leq \min\{\sqrt{\mu_1 \mu_2 / (72c_1 \mu_1 + 48)}, \sqrt{c_1 \mu_1 \mu_2^2 / 32}\}$, where $\rho = \max\{1 - \delta \mu_1 \sigma_{r^*} / 16, 1 - \tau \mu_2 / 18\} \in (0, 1)$ is a contraction parameter, and ϕ_1 and ϕ_2 are constants that depend on c_1 , c_2 , γ , μ_1 , μ_2 , α_1 and α_2 . Then for a tolerance parameter $\delta \in (0, 1)$, for any initial estimator $\{\mathbf{U}^{(0)}, \mathbf{B}^{(0)}\}$ satisfying $D\{\mathbf{U}^{(0)}, \mathbf{B}^{(0)}\} \leq c_2^2 \sigma_{r^*}$, we have,*

with probability at least $1 - \delta$,

$$D \left\{ \mathbf{U}^{(t)}, \mathbf{B}^{(t)} \right\} \leq \rho^t D \left\{ \mathbf{U}^{(0)}, \mathbf{B}^{(0)} \right\} + \frac{r^* \phi_1 \epsilon_N^2 + s^* \phi_2 \xi_N^2}{(1 - \rho) \sigma_1},$$

Note that the contraction rate ρ in Corollary 1 is defined in the same way as that in Theorem 1. In the symmetric case, the bounds for constants c_1 and c_2 are different, which leads to different bounds for the step size choices. However, given the same δ , τ , σ_{r^*} , μ_1 and μ_2 , the convergence rate for the symmetric case is the same as that for the general case.

4.2 Error Bound for a GLM Loss Function

Next we return to the GLM loss function (2) employed in our network response generalized linear model (1). Assume the parameter space for $\{\Theta, \mathbf{B}\}$ is compact. Let $\mathbf{X} \in \mathbb{R}^{N \times p}$ denote the design matrix with its i th row equal to \mathbf{x}_i^\top , $i = 1, \dots, N$. We next introduce the conditions on \mathbf{X} and the model, so that Conditions (A1)-(A4) in Section 4.1 are satisfied.

- (B1) The samples \mathbf{x}_i 's are i.i.d. from a zero-mean sub-Gaussian distribution, and the covariance matrix Σ_x satisfies that $b_l \leq \lambda_{\min}(\Sigma_x) \leq \lambda_{\max}(\Sigma_x) \leq b_u$ for some positive constants $0 < b_l \leq b_u < \infty$, where $\lambda_{\min}(\Sigma_x)$ and $\lambda_{\max}(\Sigma_x)$ denote the smallest and largest eigenvalues of Σ_x , respectively.
- (B2) The covariates are bounded by some constant $M_x > 0$, i.e., $|\mathbf{x}_{is}| \leq M_x$.
- (B3) Each element of $\mathbf{A}^{(i)}$ conditional on \mathbf{x}_i follows an exponential distribution, and the second derivative of the cumulant function $\psi''(\cdot)$ is continuous.

Condition (B1) assumes a sub-Gaussian random design, which is common in high-dimensional problems (Raskutti et al., 2011; Chen et al., 2016). Besides, our results can be analogously extended to a fixed design matrix, by explicitly specifying the conditions on \mathbf{X} . Condition (B2) is to bound the Hessian of the cumulant function in the neighborhood of \mathbf{B}^* , and is common in high-dimensional generalized linear models (Negahban et al., 2012; Chen et al., 2016). Condition (B3) is general, and is satisfied by most generalized linear models. Conditions (B2) and (B3) together imply that, for any $\Theta \in \mathbb{B}_{\Theta^*}(\sqrt{\sigma_{r^*}}/3)$ and $\mathbf{B} \in \mathbb{B}_{\mathbf{B}^*}(\sqrt{\sigma_{r^*}}/3)$, we have $\nu_0^{-2} \leq \psi''(\Theta_{jj'} + \mathbf{x}_i^\top \mathbf{B}_{jj'}) \leq \nu_0^2$ for some positive constant ν_0 . Next, we derive the error bound for the estimator $\mathbf{U}^{(t)}$ and $\mathbf{B}^{(t)}$ from Algorithm 2 at the t th iteration under the GLM loss function (2).

Theorem 2. *Suppose Conditions (B1)-(B3) hold. Then Conditions (A1)-(A4) hold, with $\mu_1 = \nu_0^{-2}$, $\mu_2 = \lambda_{\min}(\Sigma_x)/(4\nu_0^2)$, $\alpha_1 = \nu_0^2$ and $\alpha_2 = 7\lambda_{\max}(\Sigma_x)\nu_0^2/4$. Let c_1 and c_2 be constants such that $c_1 \leq \mu_1/(96\alpha_1^2)$, and $3c_1\alpha_2 \leq c_2 \leq \min\left\{1/3, \sqrt{\mu_1/(9\alpha_1/2 + 8/\mu_2)}\right\}$. Let the step sizes $\delta = c_1/\sigma_1$, $\tau = c_2/\alpha_2$, and $s = \gamma s^*$, where $\gamma \geq 1 + \{(3\alpha_2 + \mu_2 c_2)/(\mu_2 c_2)\}^2$. When $N \geq c_3(r^*n \log n + s^* \log n)$ for some constants c_3 and c_4 , for any initial estimator $\{\mathbf{U}^{(0)}, \mathbf{B}^{(0)}\}$ satisfying $D\{\mathbf{U}^{(0)}, \mathbf{B}^{(0)}\} \leq c_2^2 \sigma_{r^*}$, we have, with probability at least $1 - c_4/n$,*

$$D\{\mathbf{U}^{(t)}, \mathbf{B}^{(t)}\} \leq \rho^t D\{\mathbf{U}^{(0)}, \mathbf{B}^{(0)}\} + \tilde{\phi}_1 \frac{r^*n \log n}{N} + \tilde{\phi}_2 \frac{s^* \log n}{N}, \quad (6)$$

where $\rho = \max\{1 - \delta\mu_1\sigma_{r^*}/16, 1 - \tau\mu_2/18\} \in (0, 1)$ is a contraction parameter, and $\tilde{\phi}_1$ and $\tilde{\phi}_2$ are constants that depend on c_1 , c_2 , ν_0 , $\lambda_{\min}(\Sigma_x)$ and $\lambda_{\max}(\Sigma_x)$.

Theorem 2 verifies the linear rate of convergence of Algorithm 2, and gives an explicit form of the statistical error for the proposed estimator. In the contraction inequality (6), the term $r^*n \log n/N$ is the statistical error from the low-rank matrix estimation, which, up to a logarithmic factor, matches with the minimax lower bound for multi-response linear regression with a low-rank constraint (Raskutti et al., 2011), and the term $s^* \log n/N$ is the statistical error from the sparse tensor estimation, which matches with the minimax lower bound for sparse linear regression (Negahban et al., 2012).

Theorem 2 again offers useful guidance on the choice of the step sizes δ and τ in Algorithm 2. Their bounds hinge on ν_0 , $\lambda_{\min}(\Sigma_x)$ and $\lambda_{\max}(\Sigma_x)$. These quantities can be estimated from the data. Specifically, we estimate Σ_x by its usual sample covariance estimator, and roughly estimate ν_0 through the second derivative ψ'' that $\nu_0^{-2} \leq \psi''(\Theta_{jj'} + \mathbf{x}_i^\top \mathbf{B}_{jj'}) \leq \nu_0^2$.

4.3 Consistency of Community Detection and Edge Selection

One implication of our model is that we can recover the community structure of the nodes given the low-rank parameterization of Θ . Community detection is a fundamental and frequently studied problem in network analysis; see Goldenberg et al. (2010) for a survey. We show that our community detection solution achieves the strong consistency. Specifically, we show our solution can correctly recover the true community labels for all nodes with probability $1 - O(K/n)$, while allowing the number of communities to grow sub-linearly with n . Here K is the number of communities and n is the number of nodes in the network.

We first formally define the true underlying community structure. Based on \mathbf{U}^* from the decomposition $\Theta^* = \mathbf{U}^* \Lambda \mathbf{U}^{*\top}$, the true community structure is determined by the rows of

\mathbf{U}^* in that there are K distinct groups of rows, such that

$$\mathbf{U}^* = (\mathbf{U}_{1\cdot}^*, \dots, \mathbf{U}_{n\cdot}^*)^\top = \left(\underbrace{\mathbf{u}_1^*, \dots, \mathbf{u}_1^*}_{l \text{ nodes}}, \underbrace{\mathbf{u}_2^*, \dots, \mathbf{u}_2^*}_{l \text{ nodes}}, \dots, \underbrace{\mathbf{u}_K^*, \dots, \mathbf{u}_K^*}_{l \text{ nodes}} \right)^\top \in \mathbb{R}^{n \times r^*},$$

where $\mathbf{u}_k^* \in \mathbb{R}^{1 \times r^*}$, $k = 1, \dots, K$. Here for notational simplicity, we assume there is an equal number of nodes, $l = n/K$, in each community. Accordingly, we define the true community assignments as $\mathcal{A}_1^* := \{1, \dots, l\}, \dots, \mathcal{A}_K^* := \{n-l+1, \dots, n\}$.

We propose to recover the community labels by applying a clustering procedure, e.g., the K -means clustering, to the rows of the final estimate $\mathbf{U}^{(t)}$ obtained from Algorithm 2. We show that the resulting clustering output achieves the strong consistency, under the following regularity conditions.

(C1) Assume that $\sigma_{r^*} > c_5$ for some constant $c_5 > 0$, where σ_{r^*} is the smallest non-zero singular value of Θ^* .

(C2) Assume that $\min_{k \neq k'} \|\mathbf{u}_k^* - \mathbf{u}_{k'}^*\|_2^2 > c_6 e_0$ for some constant $c_6 > 0$, where $e_0 = \tilde{\phi}_1 r^* n \log n / N + \tilde{\phi}_2 s^* \log n / N$, and $\tilde{\phi}_1, \tilde{\phi}_2$ are defined as in Theorem 2.

Condition (C1) requires that the minimum non-zero singular value of Θ^* is bounded below by a positive constant, which is analogous to the eigen-gap condition employed in many low-rank models (Sun et al., 2017; Zhang, 2018). Condition (C2) ensures that the minimal gap between different cluster centers does not tend to zero too fast.

Theorem 3. *Suppose the conditions in Theorem 2 and (C1)-(C2) hold. Then after t iterations with $t \geq \log_\rho \left(e_0 / D\{\mathbf{U}^{(0)}, \mathbf{B}^{(0)}\} \right)$, we have, with probability at least $1 - c_4 K/n$, $\hat{\mathcal{A}}_k^{(t)} = \mathcal{A}_k^*$, for all $k = 1, \dots, K$, where c_4 is a constant defined as in Theorem 2.*

Theorem 3 shows that our community detection procedure achieves the strong consistency as long as $K = o(n)$. Our result allows K to grow at a sub-linear rate with n . For the stochastic blockmodel based community detection method in a single network setup, Gao et al. (2018) established the strong consistency when $\log(K) = o(\log(n))$, which allows K to grow at a sub-polynomial rate with n . In comparison, our result allows K to grow at the much faster sub-linear rate. This is due to that we are modeling multiple networks over the same set of nodes, which provides more information than a single network.

Another implication of our model is that we can select the network edges that are affected by the covariates based on the sparse structure of \mathbf{B} . We first state a regularity condition.

(C3) Assume that the minimal signal $\min_{ijk} |\mathbf{B}_{ijk}^*| > 2\sqrt{\sigma_1 e_0}$, where $e_0 = \tilde{\phi}_1 r^* n \log n / N + \tilde{\phi}_2 s^* \log n / N$, and $\tilde{\phi}_1, \tilde{\phi}_2$ are defined as in Theorem 2.

Condition (C3) is a minimal signal condition, which is commonly used in high-dimensional regressions (Fan et al., 2014). The next corollary establishes the variable selection consistency of the sparse tensor estimator $\mathbf{B}^{(t)}$.

Corollary 2. *Suppose the conditions in Theorem 2 and (C3) hold. Then after t iterations with $t \geq \log_p \left(e_0 / D\{\mathbf{U}^{(0)}, \mathbf{B}^{(0)}\} \right)$, we have, with probability at least $1 - c_4/n$, for any $\mathbf{B}_{ijk}^* \neq 0$, the estimate $\mathbf{B}_{ijk}^{(t)} \neq 0$, and for any $\mathbf{B}_{ijk}^* = 0$, the estimate $\mathbf{B}_{ijk}^{(t)} = 0$.*

Corollary 2 is a direct consequence of Theorem 2, and thus we omit its proof. This result has an important implication in practice, as it ensures that our model can correctly select the edges in the network that are affected by the subject covariates.

5 Simulations

We carry out intensive simulations to investigate the finite sample performance of our proposed method, and to compare with some competing solutions. We focus on the symmetric network throughout the simulations. In Section 5.1, we consider our own model (1), under varying sample sizes, ranks, and sparsity levels. In Section 5.2, we consider a model from Wang et al. (2017), where our model structure is not satisfied. In Sections 5.3 and 5.4, we further consider a stochastic blockmodel (Bickel et al., 2013), and a network latent factor model (Hoff, 2009), both of which can be viewed as special cases of our model. We skip the network latent space model due to its similarity to the network latent factor model. In general, we have found our method performs competitively in all settings, even under potential model misspecification. In all simulations, we tune the rank r and sparsity s using the eBIC criterion, with r from $\{1, 2, \dots, 20\}$, and $s = s_0 n^2 p$, with s_0 from $10^{\{-3, -2.9, \dots, 0.1, 0\}}$.

5.1 Low-Rank and Sparse Network Response Model

We first simulate binary network data from our proposed model (1), $g\{\boldsymbol{\mu}^{(i)}\} = \boldsymbol{\Theta} + \mathbf{B} \times_3 \mathbf{x}_i$, $i = 1, \dots, N$, where $g(\cdot)$ is the logit link function. We generate the covariates from the standard normal distribution, and standardize the columns of the design matrix to have zero mean and unit standard deviation. For $\boldsymbol{\Theta} = \mathbf{U}\boldsymbol{\Lambda}\mathbf{U}^\top$, we set $\boldsymbol{\Lambda}$ as an $r \times r$ identity

matrix, and generate the entries of $\mathbf{U} \in \mathbb{R}^{n \times r}$ from a standard normal distribution. For \mathbf{B} , we randomly set a proportion of its entries to be 2, and the rest to zero. Let $s_0 = s/(n^2 p)$ denote this proportion of the nonzero entries of \mathbf{B} . We set the number of nodes $n = 50$, the number of covariates $p = 10$, and vary the number of subjects $N = 200, 400$, the rank $r = 2, 5$, and the sparsity proportion $s_0 = 0.1, 0.3$, respectively.

We compare with three alternative methods. The first is the element-wise penalized GLM method of Firth (1993), which fits a penalized GLM to each entry of $\mathbf{A}_{jj'}$,

$$g \left[\mathbb{E} \left\{ \mathbf{A}_{jj'}^{(i)} | \mathbf{x}_i \right\} \right] = \Theta_{jj'} + \mathbf{B}_{jj'}^\top \mathbf{x}_i, \quad i = 1, \dots, N, \quad j, j' = 1, \dots, n,$$

with the Jeffreys invariant prior penalty. Here $\Theta_{jj'}$ is the (j, j') th entry of Θ , and $\mathbf{B}_{jj'}$ is the (j, j') th tube fiber of \mathbf{B} . This approach has been shown to be effective in reducing the small sample bias (Firth, 1993). The second method is similar to the first one, except that it uses an elastic-net penalty (Zou and Hastie, 2005), and the tuning is done through cross-validation. The third is the common and individual structure explained method proposed by Wang et al. (2017) coupled with a GLM, and the tuning is done using the elbow method as described in Wang et al. (2017).

To evaluate the estimation accuracy, we report the estimation errors, $N^{-1} \sum_{i=1}^N \|\boldsymbol{\mu}^{(i)} - \hat{\boldsymbol{\mu}}^{(i)}\|_F$, $\|\Theta - \hat{\Theta}\|_F$, and $\|\mathbf{B} - \hat{\mathbf{B}}\|_F$, where $\hat{\boldsymbol{\mu}}^{(i)} = g^{-1}(\hat{\Theta} + \hat{\mathbf{B}} \times_3 \mathbf{x}_i)$. To evaluate the edge selection accuracy, we report the F1 score calculated as $2TP/(2TP + FP + FN)$, where TP is the true positive count, FP is the false positive count, and FN is the false negative count. Since the method of Firth (1993) does not consider entry-wise sparsity, its F1 score is not reported. Since the method of Wang et al. (2017) could only estimate $\boldsymbol{\mu}^{(i)}$, the estimation errors for Θ and \mathbf{B} are not reported.

Table 1 reports the average criteria, with the standard errors in the parentheses, over 50 data replications. Our proposed method is seen to achieve the best performance among all competing methods, in terms of both estimation accuracy and selection accuracy, and this holds true for different sample sizes N , ranks r and sparsity levels s_0 . Moreover, we see the estimation error of our method decreases as N increases, or as r and s_0 decrease. Such observations agree with our theoretical results in Theorem 2.

5.2 Common and Individual Structure Explained Model

Next we consider the performance of our method under a potentially misspecified model. We simulate binary network data from the common and individual structure explained model

N	r	s_0	Method	Error of $\boldsymbol{\mu}^{(i)}$	Error of $\boldsymbol{\Theta}$	Error of $\boldsymbol{\mathcal{B}}$	F1 score
200	2	0.1	GLM _{JP}	1.106 (0.009)	47.09 (1.531)	35.09 (0.389)	-
			GLM _{EN}	1.063 (0.011)	47.50 (1.865)	28.38 (0.201)	0.709 (0.002)
			CISE	0.638 (0.001)	-	-	-
			GLSNet	0.152 (0.002)	3.49 (0.129)	25.79 (0.426)	0.964 (0.002)
	0.3	GLM _{JP}	1.101 (0.008)	45.06 (1.454)	52.53 (0.696)	-	
		GLM _{EN}	1.062 (0.008)	45.61 (1.561)	46.73 (0.345)	0.905 (0.001)	
		CISE	0.818 (0.001)	-	-	-	
		GLSNet	0.207 (0.002)	4.15 (0.175)	35.35 (0.415)	0.994 (0.001)	
	5	0.1	GLM _{JP}	1.353 (0.005)	93.38 (1.604)	35.55 (0.486)	-
			GLM _{EN}	1.328 (0.006)	94.64 (1.599)	29.40 (0.215)	0.736 (0.002)
			CISE	0.631 (0.001)	-	-	-
			GLSNet	0.154 (0.001)	6.51 (0.232)	26.86 (0.346)	0.960 (0.002)
0.3		GLM _{JP}	1.311 (0.005)	88.39 (1.648)	52.30 (0.613)	-	
		GLM _{EN}	1.287 (0.005)	87.92 (1.625)	47.63 (0.295)	0.916 (0.001)	
		CISE	0.838 (0.001)	-	-	-	
		GLSNet	0.211 (0.001)	9.79 (0.488)	37.27 (0.337)	0.981 (0.001)	
400	2	0.1	GLM _{JP}	0.774 (0.007)	39.04 (1.892)	25.05 (0.132)	-
			GLM _{EN}	0.756 (0.007)	40.58 (1.815)	18.35 (0.101)	0.700 (0.002)
			CISE	0.457 (0.001)	-	-	-
			GLSNet	0.055 (0.000)	2.44 (0.110)	13.61 (0.185)	0.997 (0.000)
	0.3	GLM _{JP}	0.769 (0.006)	36.47 (1.388)	33.27 (0.130)	-	
		GLM _{EN}	0.752 (0.006)	38.48 (1.135)	30.47 (0.117)	0.901 (0.001)	
		CISE	0.577 (0.001)	-	-	-	
		GLSNet	0.088 (0.000)	3.04 (0.131)	22.51 (0.151)	0.998 (0.000)	
	5	0.1	GLM _{JP}	0.974 (0.004)	81.80 (1.923)	26.82 (0.110)	-
			GLM _{EN}	0.964 (0.004)	82.52 (1.893)	18.86 (0.087)	0.716 (0.002)
			CISE	0.452 (0.001)	-	-	-
			GLSNet	0.061 (0.000)	4.57 (0.161)	14.97 (0.234)	0.993 (0.001)
0.3		GLM _{JP}	0.939 (0.004)	77.18 (1.466)	34.65 (0.156)	-	
		GLM _{EN}	0.927 (0.004)	77.94 (1.435)	31.13 (0.136)	0.908 (0.001)	
		CISE	0.513 (0.001)	-	-	-	
		GLSNet	0.094 (0.001)	7.87 (0.274)	25.47 (0.273)	0.995 (0.000)	

Table 1: Simulation results under the low-rank and sparse model, with the varying sample size N , rank r and sparsity proportion s_0 . The four methods under comparison are: the element-wise penalized GLM with the Jeffreys invariant prior penalty (denoted as GLM_{JP}), the element-wise penalized GLM with the elastic-net penalty (GLM_{EN}), the common and individual structure explained method (CISE), and our proposed generalized low-rank and sparse network response model (GLSNet). The standard errors are shown in the parentheses. The minimal error and maximal F1 score in each case are shown in boldface.

r	Method	$N = 200$		$N = 400$	
		Error of $\boldsymbol{\mu}^{(i)}$	Error of $\boldsymbol{\Theta}$	Error of $\boldsymbol{\mu}^{(i)}$	Error of $\boldsymbol{\Theta}$
5	CISE	0.435 (0.000)	46.08 (0.553)	0.301 (0.000)	44.74 (0.651)
	GLSNet	0.506 (0.002)	16.50 (0.256)	0.359 (0.002)	16.27 (0.289)
20	CISE	0.306 (0.000)	157.2 (1.130)	0.440 (0.000)	155.8 (1.195)
	GLSNet	0.294 (0.001)	104.8 (1.367)	0.423 (0.002)	100.6 (1.463)

Table 2: Simulation results under the common and individual structure explained model, with the varying sample size N and rank r . The two methods under comparison are: the common and individual structure explained method (CISE), and our proposed generalized low-rank and sparse network response model (GLSNet). The standard errors are shown in the parentheses.

of Wang et al. (2017),

$$g\{\boldsymbol{\mu}^{(i)}\} = \boldsymbol{\Theta} + \mathbf{D}_i, \quad i = 1, \dots, N,$$

where $g(\cdot)$ is the logit link, $\boldsymbol{\Theta}$ characterizes the common connectivity pattern, and \mathbf{D}_i represents the individual deviation. For $\boldsymbol{\Theta} = \mathbf{U}\boldsymbol{\Lambda}\mathbf{U}^\top$, we set $\boldsymbol{\Lambda}$ as an $r \times r$ identity matrix, and generate the entries of $\mathbf{U} \in \mathbb{R}^{n \times r}$ from a standard normal distribution. We set $\mathbf{D}_i = \mathbf{d}_i \circ \mathbf{d}_i$, where \circ is outer product, and generate the entries of $\mathbf{d}_i \in \mathbb{R}^n$ from a standard normal distribution. The model of Wang et al. (2017) cannot incorporate subject covariates, and hence \mathcal{B} is not included. Moreover, $\boldsymbol{\Theta} + \mathbf{D}_i$ is not necessarily a low-rank matrix. As such, our model assumption may not be satisfied. We set $n = 50$, $N = 200, 400$, and $r = 5, 20$.

Table 2 reports the estimation errors based on 50 data replications for our method and that of Wang et al. (2017). It is seen that, under this potentially misspecified model, our method still achieves a comparable performance as Wang et al. (2017).

5.3 Stochastic Blockmodel

Next we simulate data from a stochastic blockmodel (SBM), and compare our method with the variational EM method specifically designed for SBM (Bickel et al., 2013). Following the model setup in Section 2.2, given the connecting probability matrix \mathbf{M} and the community assignment matrix \mathbf{C} , we generate $\mathbf{A}_{jj'i}$'s as independent Bernoulli random variables, with $P(\mathbf{A}_{jj'i} = 1) = \mathbf{C}_{.j}\mathbf{M}\mathbf{C}_{.j'}^\top$, $i = 1, \dots, N$. We set $n = 100$ nodes, belonging to $K = 3$ communities, and the number of nodes in each community is 50, 25, and 25, respectively. This determines the community membership matrix $\mathbf{C} \in \mathbb{R}^{n \times K}$, whose entries are 0 or 1. We set the connecting probability matrix \mathbf{M} as a 3×3 matrix, with w on the diagonal

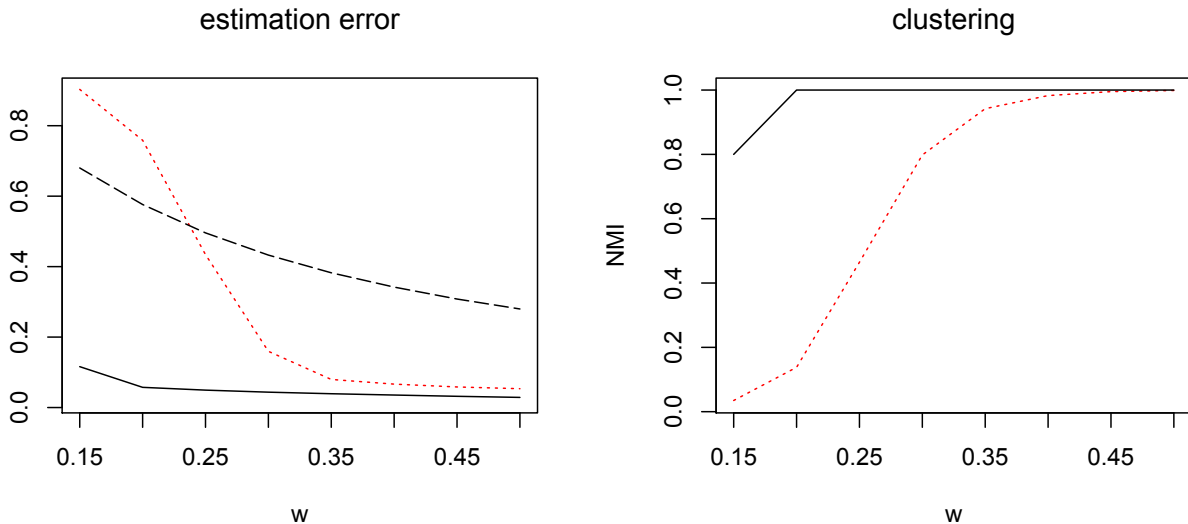


Figure 1: Simulation results under the stochastic blockmodel, with the varying signal strength w . The left panel reports the average estimation error, and the right panel reports the average clustering accuracy. The three methods under comparison are: the variational EM method (red dotted line), the common and individual structure explained method of Wang et al. (2017) (black dashed line), and our generalized low-rank and sparse network response model (black solid line).

representing the within-community connecting probability, and 0.1 on the off-diagonal representing the between-community connecting probability. We vary the value of w from 0.15 to 0.50, with a larger value of w implying a larger difference between the within-community and the between-community connecting probabilities, and thus a stronger signal. Since the classical SBM has been designed for a single network, it does not incorporate the subject covariates. Moreover, it usually assumes the number of communities K is known. As such, we set K at the true value for all estimation methods. We generate $N = 100$ networks. We fit the stochastic blockmodel to each of the N networks, and report the average estimates.

To evaluate the estimation accuracy, we report the normalized estimation error, $N^{-1} \sum_{i=1}^N \|\boldsymbol{\mu}^{(i)} - \hat{\boldsymbol{\mu}}^{(i)}\|_F / \|\boldsymbol{\mu}^{(i)}\|_F$. To evaluate the node clustering accuracy, we report the normalized mutual information between the estimated clustering membership and the true membership. Figure 1 reports the average results based on 50 data replications. We also include the method of Wang et al. (2017) in the comparison, but only report its estimation error, as it cannot produce any community estimation. It is seen that our method outperforms the variational EM method in both estimation accuracy and clustering accuracy. This is because

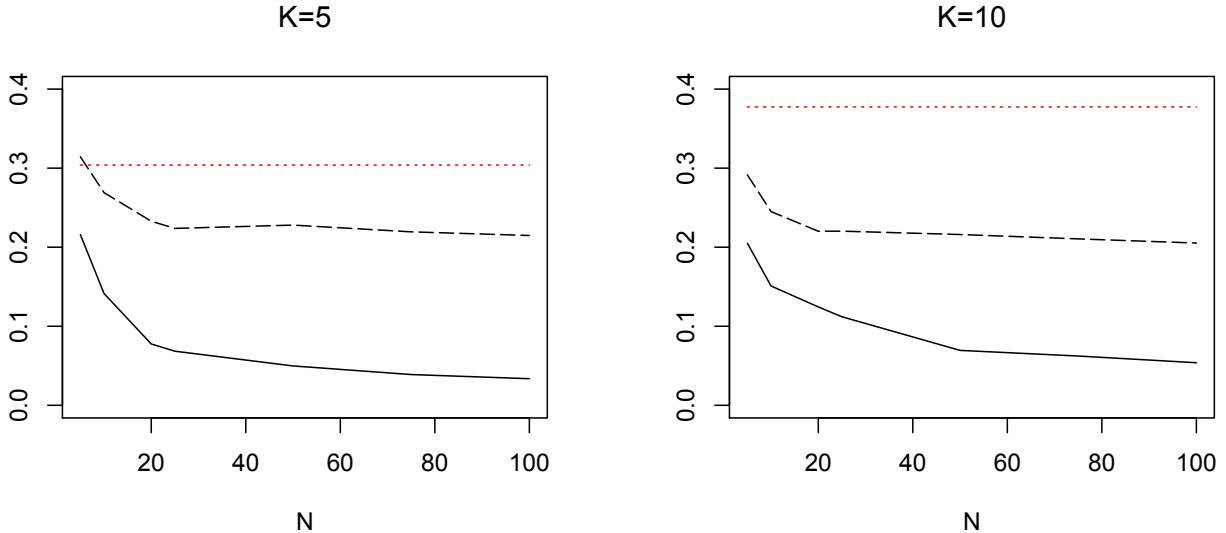


Figure 2: Simulation results under the latent factor model, with the varying sample size N and number of latent factors K . The left panel reports the average estimation error for $K = 5$, and the right panel for $K = 10$. The three methods under comparison are: the Bayesian MCMC method (red dotted line), the common and individual structure explained method of Wang et al. (2017) (black dashed line), and our proposed generalized low-rank and sparse network response model (black solid line).

our method utilizes information from all N subjects jointly, whereas the variational EM method utilizes each subject’s information separately, and only averages the estimates in the final step. This difference is more pronounced when the signal strength is relatively weak, such as when w is smaller than 0.3. The superior empirical clustering accuracy also agrees with our theoretical findings in Theorem 3.

5.4 Network Latent Factor Model

Finally, we simulate data from the network latent factor model, and compare our method with the Bayesian MCMC method (Minhas et al., 2016). Again, following the model setup in Section 2.2, we simulate the node additive effect α_j and the node multiplicative effect \mathbf{c}_j , $1 \leq j \leq n$, from the standard normal distribution. We set the number of latent factors $K = 5, 10$, and vary the sample size N from 5 to 100. Similar as in Section 5.3, the subject covariates are not incorporated, and the Bayesian MCMC method is applied to each sample separately, then the results are averaged. The method of Wang et al. (2017) is also included

in the comparison. Figure 2 reports the normalized estimation error averaged over 50 data replications. It is seen again that our method performs best, as it jointly models all N samples and effectively borrows information from each other. As the sample size N increases, the estimation error of our method decreases. As the number of latent factors K increases, the rank of the low-rank representation increases and the estimation error increases. These observations agree with our theoretical results in Theorem 2.

6 Applications to Brain Connectivity Analysis

We applied the proposed method to two brain connectivity studies. The first is a study of functional connectivity, which is based on resting-state functional magnetic resonance imaging (fMRI), and the corresponding network edge is a 0/1 indicator resulting from a thresholded precision matrix. The second is a study of structural connectivity, which is based on diffusion tensor imaging (DTI), and the corresponding network edge is the count of white matter fibers between pairs of brain regions.

6.1 Functional Connectivity Analysis

We first analyzed a resting-state fMRI dataset from ADHD-200 (http://fcon_1000.projects.nitrc.org/indi/adhd200/). We focused on $N = 319$ healthy control subjects, aging between 7.09 to 21.8 years old, with 46.4% females and 53.6% males. Each subject received a resting-state fMRI scan, and the image was preprocessed, including slice timing correction, motion correction, spatial smoothing, denoising by regressing out motion parameters, white matter, and cerebrospinal fluid time, and band-pass filtering. Each fMRI image was then summarized in the form of a binary network, with the nodes corresponding to 264 seed regions of interest in the brain based on a cortical parcellation system defined by Power et al. (2011), and the edges recording the binary indicator of the thresholded partial correlations between pairs of those 264 nodes. See Zhang et al. (2018a) for more information about data collection and processing. We applied our network response model to this data with a logit link function. We standardized the covariates, age and sex, to have mean zero and variance one. We selected the rank $r = 9$ and the sparsity proportion $s_0 = 0.02$ based on eBIC.

We first examine the estimate $\hat{\Theta}$. In the neuroscience literature, those 264 nodes have been partitioned into 10 functional modules (Smith et al., 2009). Each module possesses

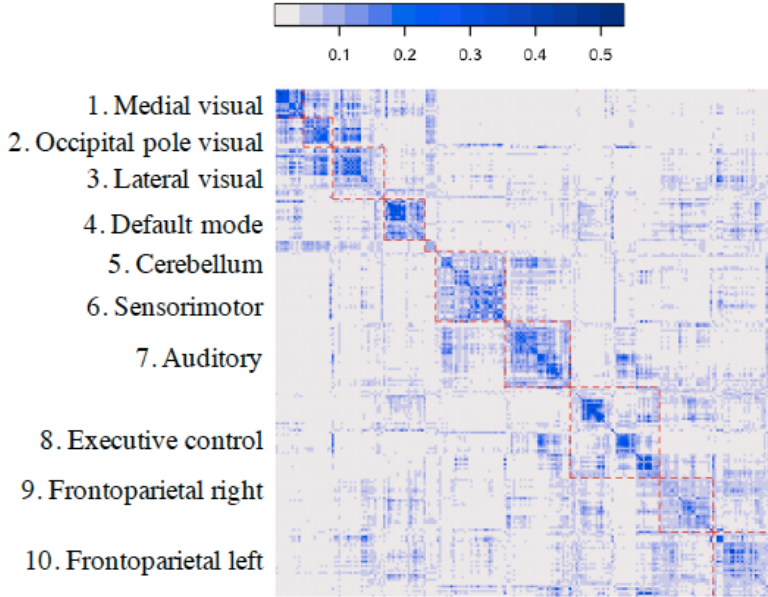


Figure 3: The functional connectivity study. Heatmap of the 264×264 matrix $g^{-1}(\hat{\Theta})$ with rows and columns ordered according to the pre-specified functional module membership. The red dashed lines mark the boundaries of the ten functional modules.

a relatively autonomous functionality, and complex brain tasks are carried out through coordinated collaborations among those modules. Figure 3 shows the heatmap of $g^{-1}(\hat{\Theta})$, with the nodes ordered according to the functional modules. Here the function $g^{-1}(\cdot)$ maps a value from the real line to $[0, 1]$ so to facilitate data visualization. From this figure, we see that our estimate agrees reasonably well with the pre-specified functional modules by Smith et al. (2009). We observe larger values of $\hat{\Theta}$ located within the diagonal blocks, which indicates a higher functional connectivity within those functional modules. Furthermore, there are high connectivities among modules 1-3, namely, the medial visual, occipital pole visual and lateral visual modules. The medial and occipital visual modules are important in both simple visual stimuli, e.g., a flickering checkerboard, and higher-order visual stimuli, e.g., orthography. The lateral visual network is important in complex emotional stimuli (Laird et al., 2011). These visual modules appear to have high connectivities with the cerebellum, but generally low connectivities with the rest of functional modules. We also observe a high connectivity between modules 9-10, namely, the frontoparietal right and frontoparietal left

modules. These two modules are important in attention control and can generate a diverse range of control signals depending on task demands (Scolari et al., 2015).

We next examine the estimate $\hat{\mathcal{B}}$. In $\hat{\mathcal{B}}_{..1}$, i.e., the coefficient matrix for the sex covariate, the non-sparse entries are located within the lateral visual module and the entries values are negative, ranging from -0.777 to -0.506 . This indicates that male subjects have lower connectivities in those regions within the lateral visual module. The non-sparse entries of $\hat{\mathcal{B}}$ mostly concentrate in $\hat{\mathcal{B}}_{..2}$, i.e., the coefficient matrix for the age covariate. In $\hat{\mathcal{B}}_{..2}$, the positive entries are located within the occipital pole visual, default mode, executive control and frontoparietal left modules, with values ranging from 0.454 to 0.902 . This indicates that the connectivities within those modules increase with age. We also observe positive entries located in default model to executive control, default model to frontoparietal right and executive control to both frontoparietal right and left modules, with values ranging from 0.465 to 0.771 . In $\hat{\mathcal{B}}_{..2}$, the negative entries are located within the lateral visual module, sensorimotor and auditory modules, with values ranging from -1.097 to -0.536 . This indicates that the connectivities within those modules decrease with age. We also find negative entries located in medial visual to lateral visual, executive control to frontoparietal right and default mode to auditory modules, with values ranging from -1.350 to -1.095 . This indicates that the connectivities between those modules also decrease with age. These findings suggest some interesting patterns that warrant further investigation and verification.

6.2 Structural Connectivity Analysis

We next analyzed a structural DTI dataset from KKI-42 (<http://openconnecto.me/data/public/MR/archive/>). We focused on 21 subjects with no history of neurological conditions, aging from 22 to 61 years old, with 47.6% females and 52.4% males. Each subject received a resting-state DTI scan, which was a magnetic resonance imaging technique that enables measurement of the diffusion of water in order to produce neural tract images. Estimates of white matter connectivity patterns can be obtained using the diffusion anisotropy and the principal diffusion directions. In the KKI-42 study, a scan-rescan imaging session was conducted on each subject, leading to two images for each subject and a total of $N = 42$ for the study. For simplicity, we treated those images as if they formed independent samples. Each DTI image was preprocessed, and was summarized in the form of a count network, with $n = 68$ nodes defined following the Desikan Atlas that are equally divided in left and right hemispheres (Desikan et al., 2006), and the edges recording the total number

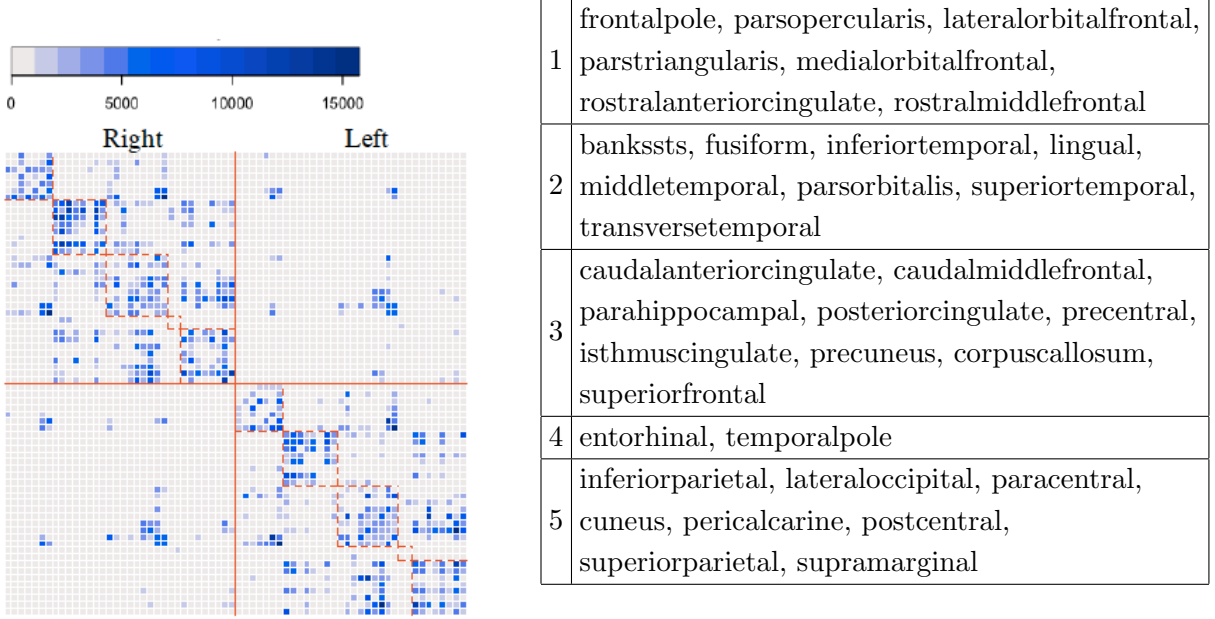


Figure 4: The structural connectivity study. Left panel: heatmap of the 68×68 matrix $g^{-1}(\hat{\Theta})$ with rows and columns ordered according to the K -means clustering result. Right and left hemispheres are marked in the plot. The red dashed lines mark the boundaries of the identified groups. Right panel: anatomic regions of interest in the identified groups.

of white matter fibers between the pair of nodes. See Landman et al. (2011) for more information about data collection, and Roncal et al. (2013) for details on the construction of brain network from DTI scans. We applied our network response model to this data, with a log link function. We standardized the covariates, age and sex, to have mean zero and variance one. We selected the rank $r = 5$ and the sparsity proportion $s_0 = 0.31$.

We first examine the estimate $\hat{\Theta}$. To the best of our knowledge, communities in structural connectivity networks have not been studied before. We applied the K -means clustering algorithm to the estimate $U^{(t)}$ from $\hat{\Theta}$, and identified five clusters among the 68 anatomic regions of interest (ROIs). We selected the number of clusters based on the elbow plot. Figure 4, right panel, reports the members of each cluster in the table. From an anatomical perspective, the first group of nodes are entirely contained in the frontal lobe, the second group are mostly contained in the temporal lobe, the fourth group are entirely contained in the temporal lobe, and the third and fifth groups contain nodes from the frontal, parietal, occipital and temporal lobes. Many of the 68 anatomic ROIs in the Desikan Atlas overlap with the resting state functional modules (Kabbara et al., 2017). By exploring this overlap, we gained further insights of potential functions of those five groups. We found that group

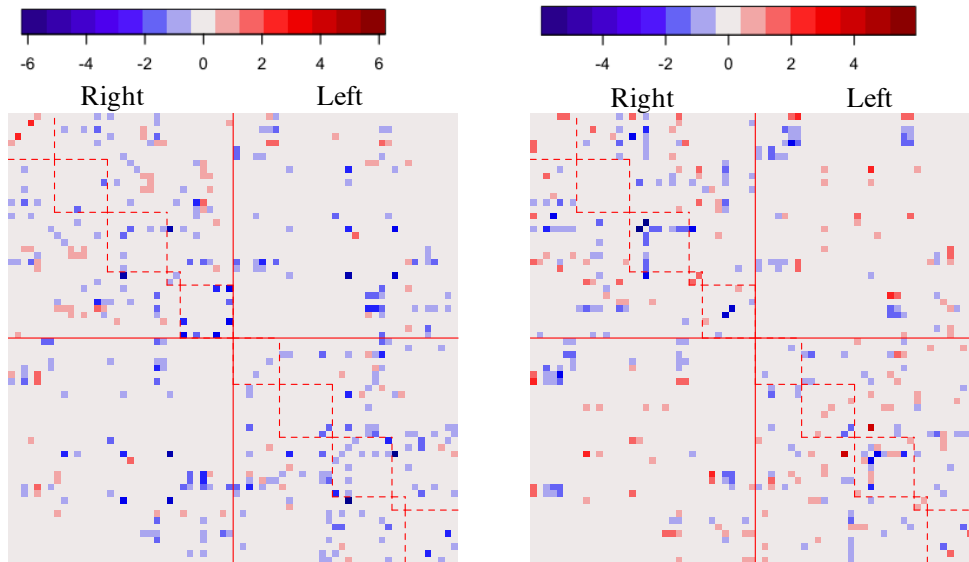


Figure 5: The structural connectivity study. Left panel: the age coefficient matrix. Right panel: the sex coefficient matrix.

1 is related to dorsal attention and default mode, group 2 is related to visual and auditory, group 3 is related to default mode, and group 5 is related to visual. The resting state functions of nodes in Groups 4 are unidentified. Figure 4, left panel, shows the heatmap of the estimated $\hat{\Theta}$ with nodes reordered according to the cluster membership. Within each hemisphere, there are high structural connectivities within the identified groups. Moreover, there is a high connectivity between Groups 3 and 5. Between the two hemispheres, there are generally very low structural connectivities, while part of Group 3 from left and right hemispheres appear to have a high connectivity.

We next examine the estimate $\hat{\mathcal{B}}$. Figure 5 shows the estimated subject covariates effect coefficients. From the left panel of Figure 5, we see that, as age increases, the structural connectivity generally decreases both within and between the two hemispheres. This result agrees with existing neurological finding (Betz et al., 2014). From the right panel of Figure 5, we see that male and female subjects have different structural connectivity patterns. Such differences are observed in the between-group connections within and between hemispheres, and in the within-group connections within each hemisphere. For instance, we see males have a lower between-hemisphere connectivity for ROIs in Group 1. This observation

agrees with the existing literature that males have a lower connectivity between the left and right frontal regions (Ingalhalikar et al., 2014).

References

- Airoldi, E. M., Blei, D. M., Fienberg, S. E., and Xing, E. P. (2008), “Mixed membership stochastic blockmodels,” *Journal of Machine Learning Research*, 9, 1981–2014.
- Betzler, R. F., Byrge, L., He, Y., Goñi, J., Zuo, X.-N., and Sporns, O. (2014), “Changes in structural and functional connectivity among resting-state networks across the human lifespan,” *Neuroimage*, 102, 345–357.
- Bickel, P., Choi, D., Chang, X., and Zhang, H. (2013), “Asymptotic Normality of Maximum Likelihood and its Variational Approximation for Stochastic Blockmodels,” *Annals of Statistics*, 41, 1922–1943.
- Bullmore, E. and Sporns, O. (2009), “Complex brain networks: graph theoretical analysis of structural and functional systems,” *Nature Reviews Neuroscience*, 10, 186–198.
- Burer, S. and Monteiro, R. D. (2003), “A nonlinear programming algorithm for solving semidefinite programs via low-rank factorization,” *Mathematical Programming*, 95, 329–357.
- Chen, H., Raskutti, G., and Yuan, M. (2016), “Non-Convex Projected Gradient Descent for Generalized Low-Rank Tensor Regression,” *arXiv preprint arXiv:1611.10349*.
- Chen, J. and Chen, Z. (2012), “Extended BIC for small-n-large-P sparse GLM,” *Statistica Sinica*, 555–574.
- Desikan, R. S., Ségonne, F., Fischl, B., Quinn, B. T., Dickerson, B. C., Blacker, D., Buckner, R. L., Dale, A. M., Maguire, R. P., Hyman, B. T., et al. (2006), “An automated labeling system for subdividing the human cerebral cortex on MRI scans into gyral based regions of interest,” *Neuroimage*, 31, 968–980.
- Durante, D., Dunson, D. B., and Vogelstein, J. T. (2017), “Nonparametric Bayes modeling of populations of networks,” *Journal of the American Statistical Association*, 112, 1516–1530.
- Fan, J., Xue, L., and Zou, H. (2014), “Strong oracle optimality of folded concave penalized estimation,” *Annals of Statistics*, 42, 819.
- Firth, D. (1993), “Bias reduction of maximum likelihood estimates,” *Biometrika*, 80, 27–38.
- Gao, C., Ma, Z., Zhang, A. Y., and Zhou, H. H. (2018), “Community detection in degree-corrected block models,” *The Annals of Statistics*, 46, 2153–2185.
- Goldenberg, A., Zheng, A. X., Fienberg, S. E., and Airoldi, E. M. (2010), “A survey of statistical network models,” *Foundations and Trends® in Machine Learning*, 2, 129–233.

- Hoff, P. D. (2009), “Multiplicative latent factor models for description and prediction of social networks,” *Computational and mathematical organization theory*, 15, 261.
- Hoff, P. D., Raftery, A. E., and Handcock, M. S. (2002), “Latent space approaches to social network analysis,” *Journal of the American Statistical Association*, 97, 1090–1098.
- Holland, P. W., Laskey, K. B., and Leinhardt, S. (1983), “Stochastic blockmodels: First steps,” *Social Networks*, 5, 109 – 137.
- Huang, S. and Feng, Y. (2018), “Pairwise Covariates-adjusted Block Model for Community Detection,” *arXiv preprint arXiv:1807.03469*.
- Ingalhalikar, M., Smith, A., Parker, D., Satterthwaite, T. D., Elliott, M. A., Ruparel, K., Hakonarson, H., Gur, R. E., Gur, R. C., and Verma, R. (2014), “Sex differences in the structural connectome of the human brain,” *Proceedings of the National Academy of Sciences*, 111, 823–828.
- Kabbara, A., Falou, W. E., Khalil, M., Wendling, F., and Hassan, M. (2017), “The dynamic functional core network of the human brain at rest,” *Scientific reports*, 7, 2936.
- Kim, B., Lee, K., Xue, L., and Niu, X. (2017), “A Review of Dynamic Network Models with Latent Variables,” *arXiv preprint arXiv:1711.10421*.
- Kolaczyk, E. D. (2009), *Statistical Analysis of Network Data: Methods and Models*, Springer.
- Laird, A. R., Fox, P. M., Eickhoff, S. B., Turner, J. A., Ray, K. L., McKay, D. R., Glahn, D. C., Beckmann, C. F., Smith, S. M., and Fox, P. T. (2011), “Behavioral interpretations of intrinsic connectivity networks,” *Journal of cognitive neuroscience*, 23, 4022–4037.
- Landman, B. A., Huang, A. J., Gifford, A., Vikram, D. S., Lim, I. A. L., Farrell, J. A., Bogovic, J. A., Hua, J., Chen, M., Jarso, S., et al. (2011), “Multi-parametric neuroimaging reproducibility: a 3-T resource study,” *Neuroimage*, 54, 2854–2866.
- McCullagh, P. and Nelder, J. A. (1989), *Generalized linear models*, vol. 37, CRC press.
- Minhas, S., Hoff, P. D., and Ward, M. D. (2016), “Inferential Approaches for Network Analyses: AMEN for Latent Factor Models,” *arXiv preprint arXiv:1611.00460*.
- Negahban, S. N., Ravikumar, P., Wainwright, M. J., and Yu, B. (2012), “A unified framework for high-dimensional analysis of M -estimators with decomposable regularizers,” *Statistical Science*, 27, 538–557.
- Park, D., Kyrillidis, A., Caramanis, C., and Sanghavi, S. (2016), “Non-square matrix sensing without spurious local minima via the Burer-Monteiro approach,” *arXiv preprint arXiv:1609.03240*.
- Paul, S. and Chen, Y. (2016), “Consistent community detection in multi-relational data through restricted multi-layer stochastic blockmodel,” *Electronic Journal of Statistics*, 10, 3807–3870.

- Power, J. D., Cohen, A., Nelson, S., Wig, G. S., Barnes, K., Church, J., Vogel, A., Laumann, T., Miezin, F., Schlaggar, B., and Petersen, S. (2011), “Functional Network Organization of the Human Brain,” *Neuron*, 72, 665–78.
- Raskutti, G., Wainwright, M. J., and Yu, B. (2011), “Minimax rates of estimation for high-dimensional linear regression over ℓ_q -balls,” *IEEE transactions on information theory*, 57, 6976–6994.
- Roncal, W. G., Koterba, Z. H., Mhembere, D., Kleissas, D. M., Vogelstein, J. T., Burns, R., Bowles, A. R., Donavos, D. K., Ryman, S., Jung, R. E., et al. (2013), “MIGRAINE: MRI graph reliability analysis and inference for connectomics,” *Global Conference on Signal and Information Processing*, 313–316.
- Salter-Townshend, M. and McCormick, T. H. (2017), “Latent space models for multiview network data,” *The annals of applied statistics*, 11, 1217.
- Scolari, M., Seidl-Rathkopf, K. N., and Kastner, S. (2015), “Functions of the human frontoparietal attention network: Evidence from neuroimaging,” *Current opinion in behavioral sciences*, 1, 32–39.
- Sewell, D. K. and Chen, Y. (2015), “Latent space models for dynamic networks,” *Journal of the American Statistical Association*, 110, 1646–1657.
- Smith, S. D., Fox, P. T., Miller, K., Glahn, D., Fox, P., Mackay, C. E., Filippini, N., Watkins, K. E., Toro, R., Laird, A., and Beckmann, C. F. (2009), “Correspondence of the brain; functional architecture during activation and rest.” *Proceedings of the National Academy of Sciences of the United States of America*, 106, 13040–5.
- Sun, W. and Li, L. (2017), “STORE: Sparse Tensor Response Regression and Neuroimaging Analysis,” *Journal of Machine Learning Research*, 18, 4908–4944.
- Sun, W., Lu, J., Liu, H., and Cheng, G. (2017), “Provable Sparse Tensor Decomposition,” *Journal of the Royal Statistical Society, Series B*, 79, 899–916.
- Supekar, K., Uddin, L. Q., Khouzam, A., Phillips, J., Gaillard, W. D., Kenworthy, L. E., Yerys, B. E., Vaidya, C. J., and Menon, V. (2013), “Brain hyperconnectivity in children with autism and its links to social deficits,” *Cell reports*, 5, 738–747.
- Varoquaux, G. and Craddock, R. C. (2013), “Learning and comparing functional connectomes across subjects,” *NeuroImage*, 80, 405 – 415.
- Vounou, M., Nichols, T. E., Montana, G., and Initiative, A. D. N. (2010), “Discovering genetic associations with high-dimensional neuroimaging phenotypes: a sparse reduced-rank regression approach,” *Neuroimage*, 53, 1147–1159.
- Wang, L., Zhang, Z., and Dunson, D. (2017), “Common and individual structure of multiple networks,” *arXiv preprint arXiv:1707.06360*.

- Wang, Z., Gu, Q., Ning, Y., and Liu, H. (2015), “High Dimensional EM Algorithm: Statistical Optimization and Asymptotic Normality,” in *Advances in Neural Information Processing Systems*.
- Wang, Z., Liu, H., and Zhang, T. (2014), “Optimal computational and statistical rates of convergence for sparse nonconvex learning problems,” *Annals of Statistics*, 2164–2201.
- Zhang, A. (2018), “Cross: Efficient Low-rank Tensor Completion,” *Annals of Statistics*, To Appear.
- Zhang, A. and Han, R. (2018), “Optimal Sparse Singular Value Decomposition for High-dimensional High-order Data,” *Journal of the American Statistical Association*, To Appear.
- Zhang, J., Sun, W. W., and Li, L. (2018a), “Mixed-Effect Time-Varying Network Model and Application in Brain Connectivity Analysis,” *arXiv preprint arXiv:1806.03829zhang2018mixedge*.
- Zhang, X., Wang, L., and Gu, Q. (2018b), “A Unified Framework for Nonconvex Low-Rank plus Sparse Matrix Recovery,” in *International Conference on Artificial Intelligence and Statistics*, pp. 1097–1107.
- Zhang, Y., Levina, E., Zhu, J., et al. (2016), “Community detection in networks with node features,” *Electronic Journal of Statistics*, 10, 3153–3178.
- Zhang, Z., Allen, G. I., Zhu, H., and Dunson, D. (2018c), “Tensor network factorizations: Relationships between brain structural connectomes and traits,” *arXiv preprint arXiv:1806.02905*.
- Zhao, Y. (2017), “A survey on theoretical advances of community detection in networks,” *Wiley Interdisciplinary Reviews: Computational Statistics*, 9, e1403.
- Zhao, Y., Levina, E., and Zhu, J. (2012), “Consistency of community detection in networks under degree-corrected stochastic block models,” *Annals of Statistics*, 40, 2266–2292.
- Zheng, Q. and Lafferty, J. (2016), “Convergence analysis for rectangular matrix completion using Burer-Monteiro factorization and gradient descent,” *arXiv preprint arXiv:1605.07051*.
- Zhou, H., Li, L., and Zhu, H. (2013), “Tensor regression with applications in neuroimaging data analysis,” *Journal of the American Statistical Association*, 108, 540–552.
- Zou, H. and Hastie, T. (2005), “Regularization and variable selection via the elastic net,” *Journal of the Royal Statistical Society: Series B (Statistical Methodology)*, 67, 301–320.